Frustrated coupling based adiabatic coupler

by

Josep Maria Fargas Cabanillas

B.S., Universitat Politecnica de Catalunya, 2016

A thesis submitted to the

Faculty of the Graduate School of the

University of Colorado in partial fulfillment

of the requirements for the degree of

Master of science

Department of Electrical, Computer, and Energy Engineering

2017

This thesis entitled:
Frustrated coupling based adiabatic coupler
written by Josep Maria Fargas Cabanillas
has been approved for the Department of Electrical, Computer, and Energy Engineering

_____

Prof. Milos Popovic

_____

Prof. Anatoly Khilo

_____

Prof. Kelvin Wagner

Date _____

The final copy of this thesis has been examined by the signatories, and we find that both the content and the form meet acceptable presentation standards of scholarly work in the above mentioned discipline.

Fargas Cabanillas, Josep Maria (M.S., Electrical engineering)

Frustrated coupling based adiabatic coupler

Thesis directed by Prof. Milos Popovic

In this master thesis we will present a new type of 2x2 3dB coupler that we called frustrated coupling based adiabatic coupler. In our knowledge this coupler has the best performance among all the 2x2 3dB 220nm thick silicon couplers. It has a splitting ratio of at least 51/49 over 200nm bandwidth. Also 0.11dB splitting ratio over 40nm bandwidth. Low loss under 2.5% over the 200nm and under 1% on the 40 bandwidth. Finally its footprint is 3.6m x 28m. It is 5 times smaller than the best MMI [3].

Dedication

Dedicated to my brother and sister: Dani and Gemma

Acknowledgements

First of all I want to acknowledge all the people that helped me and support me in this journey. Specially, I want to thank my advisor Prof. Milos Popovic for his guidance during my project. I would like to acknowledge all the members and exmembers of the lab, Imbert, Yangyang, Savvy, Mark, Nathan, Yossi, Hayk, Bohan and specially Cale. Thank you Cale for helping me and for your patience solving all my questions. I would like to say thank you to my family an my friends in Boulder specially to my roomies; Alberto,Savina and Juan to give me support every day. Finally I will like to acknowledge my sponsors: Fundacio Balsells, Nanophotonics LAB. With out their founding this adventure would haven't been possible.

Contents

Chapter

Tables

Table

Figures

Figure

Chapter 1

Introduction

On the late 1960's integrated photonics was born. On Miller's original paper we can find what it has been the core concepts of integrated photonics [7]. Silicon-on-insulator (SOI) is one branch of integrated photonics that uses silicon as the main material to guide light. A high index contrast between silicon and normally silicon oxide allows the creation of waveguides. And Thus those lead to couplers, gradings, modulators etc. This technology was born mainly as a byproduct of electronic chips foundries. Optics engineers realized that they could use SOI to create photonics chips. This platform is increasingly becoming more and more popular due to its compactness and scalability.

Silicon phototonics systems are made of different structures that manipulate light in different ways. The most basic structure is the waveguide that allows to propagate the light though the photonic chip. An other interesting structure is a 2x2 coupler. This device has two inputs and two outputs and splits the light from each input to the two outputs evenly. It can seem that is a trivial device but the 2x2 coupler is key to built most of the silicon photonics systems. For example to build a Mach-Zender interferometer we need two 2x2 couplers. Boson sampling and linear quantum integrated photonics are good examples where 2x2 couplers are need.

In this thesis we will explore the main approaches to design a 2x2 coupler and we will present a novel 2x2 coupler design which we called frustrated coupling based adiabatic coupler.

Chapter 2

Theory to descrive 2x2 couplers

In this chapter we are going to explore the theory to understand the different kinds of 2x2 couplers in the literature. In order to do that first, we are going to introduce the slab waveguide to understand the basic concepts. Then we will present a three dimensional waveguide and it's properties. After understanding waveguides we are going to introduce coupled mode theory, supermode picture and adiabatic theory to be able to describe property the different type of couplers.

2.1   Slab waveguide

Firstly we want to introduce the concept of optical guidance. Imagine a long square metallic pipe made of metal with air inside. If an electromagnetic wave gets into the pipe it will hit the walls and reflect as in a mirror and hit an other wall and reflect again and so on. Then we can say that the square metallic pipe is guiding the electromagnetic wave. However we are working with optical frequencies and metal generates high losses at those frequencies. But we can use the same idea to guide optical frequencies.

The simplest optical waveguide is the dielectric slab. Is one of the few structures which can be solved analytically. Understanding the slab waveguide is really useful to understand three dimensional waveguides.

The major phenomenon that makes slab waveguides work is the total internal reflection.

This happens in the interface between two dielectrics if the indecent angle is small enough. From geometrical optics we know that a ray of light will follow the Snell's law while crossing interface separating two different dielectrics.

$$n_1 sin(\Theta_1) = n_3 sin(\Theta_3) \tag{2.1}$$
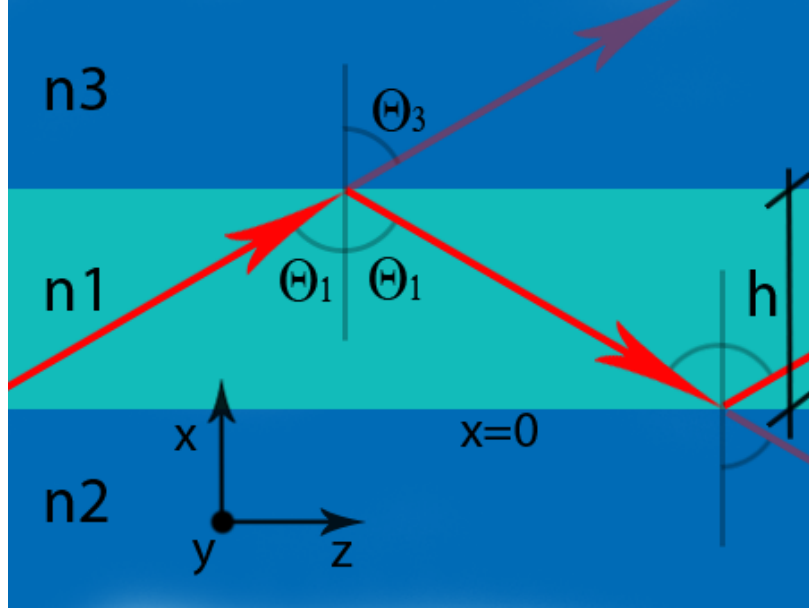
Figure 2.1: In this figure we can see the slab waveguide geometry. It consist in three layers of different dielectrics which their respective refractive indexes. Red arrows represent a ray traveling through the structure.

We define the critical angle Θ_c as the angle just before internal reflection. So the condition for the critical angle is $\Theta_3 = \pi/2$.

$$\Theta_c = asin(\frac{n_3}{n_1}) \tag{2.2}$$

Then all the waves with incident angles $\Theta_1 > \Theta_c$ will be guided due to internal reflection.

To understand the shape of the electric fields that propagate inside the structure we can simply solve Maxwell equations.

$$\nabla \times \mathbf{E}(\mathbf{r}, \mathbf{t}) = -\mu_0 \frac{\partial \mathbf{H}(\mathbf{r}, t)}{\partial t}$$
$$\nabla \times \mathbf{H}(\mathbf{r}, \mathbf{t}) = \epsilon_o n^2(\mathbf{r}) \frac{\partial \mathbf{E}(\mathbf{r}, t)}{\partial t}$$

(2.3)

The cross indicates a vector product, $\mathbf{H}$ and $\mathbf{E}$ are the magnetic and electric field vectors, and ϵ_o and μ_o are the dielectric permeability and magnetic permeability of vacuum. Magnetic and conductive materials are not considered. The index of refraction of the medium is designated by n, and t is the time.

For the slab waveguide we can assume that there is no variation in y direction so

$$\frac{\partial}{\partial y} = 0$$

(2.4)

We look for solutions with a constant propagation constant along z. For simplicity and without losing generality we are assuming polarization in y direction. So, he mode is Transverse Electric (**TE**). The other polarization: Transverse Magnetic (**TM**) can be solved analogously. Manipulating Maxwell equations we find the scalar equation that has to be satisfied on each layer.

$$\nabla^2 E_{yi}(x, z) + n_i^2 k_o^2 E_{yi}(x, z) = 0 \quad (i = 1, 2, 3)$$

(2.5)

We will to try the following solution where β is the propagation constant.

$$E_{yi}(x, z) = E_i(x) exp(-j\beta z) \quad (i = 1, 2, 3)$$

(2.6)

And then we will have to solve the following equation to find the possible values of β

$$\frac{d^2 E_i}{dx^2} + [n_i^2 k_o^2 - \beta^2] E_i = 0$$

(2.7)

We are looking for confined fields within the guide. This means we will have a standing wave

inside the guiding layer and an evanescent field outside. So, we can write.

$$\text{In layer 1: } E_1 = Ecos(\kappa x - \phi)$$

$$\text{In layer 2: } E_2 = E'exp(\gamma x) \tag{2.8}$$

$$\text{In layer 3: } E_3 = E''exp(-\delta(x - h))$$

where the constants κ,γ and δ are given by

$$\kappa = \sqrt{n_1^2 k_o^2 - \beta^2}$$

$$\gamma = \sqrt{\beta^2 - n_2^2 k_o^2} \tag{2.9}$$

$$\delta = \sqrt{\beta^2 - n_3^2 k_o^2}$$

The boundary conditions have to be satisfied. This means continuity of $E_i(x)$ and its gradient $\frac{dE_i}{dx}$ at each interface. At x=0 we get

$$E' = Ecos(\phi)$$

$$\gamma E' = -\kappa Esin(-\phi) \tag{2.10}$$

which leads to a closed-form expression for ϕ

$$tan(\phi) = \frac{\gamma}{\kappa} \tag{2.11}$$

Similarly at x=h we get

$$E'' = Ecos(\kappa h - \phi)$$

$$-\delta E'' = -\kappa Esin(\kappa h - \phi) \tag{2.12}$$

and therefore:

$$tan(\kappa h - \phi) = \frac{\delta}{\kappa} \tag{2.13}$$

Then manipulating both expressions we will finally get the dispersion relation for the slab wave guide:

$$tan(\kappa h) = \kappa\frac{\gamma + \delta}{\kappa^2 - \gamma\delta} \tag{2.14}$$

This equation has a solution for a discrete set of β. We can solve this equation 2.14 numerically and find the possible values for β. Setting the width as a variable we will obtain the dispersion curve shown in Figure 2.2.

Every mode has a different propagation constant. We know that the phase velocity is simply the speed of light over the refractive index. So we define the effective refractive index for each mode as:

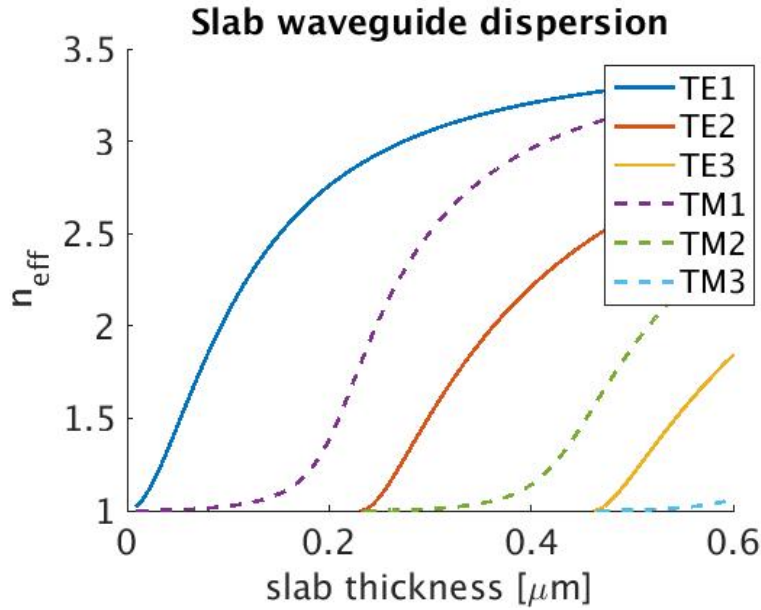$$n_{eff} = \frac{\beta_n}{k_o} = \frac{\beta_n \lambda}{2\pi} \tag{2.15}$$

Figure 2.2: In this figure we can see how the propagation constant is changing with width for both polarizations. For each with exist a set of possible modes propagating through the dielectric. The Y-axis is in units of n_{eff}. This is directly related to the propagation constant: $n_{eff} = \frac{\beta}{k_o}$. In this structure $n1 = 3.47$ (Si) ,$n2 = n3 = 1$ (Air) @1550nm

As we can see in Figure 2.2 if the slab thickness is less than $0.2\mu m$ we will have only one mode in each polarization. The first mode is called fundamental mode. A waveguide that only guides the

fundamental mode is called monomode waveguide. In future steps we will like to have monomode waveguides. It can be proven that the set of modes is complete. Every mode is perpendicular respect to the others and the set of all of them form a base. This condition implies that the overlap integral over the volume for the product of the electric field of two modes i and j is δ_{ij}. The number of nulls depends on the order of mode. For example the fundamental mode does not have any null. The first mode has a null, the second has two and so on [11].
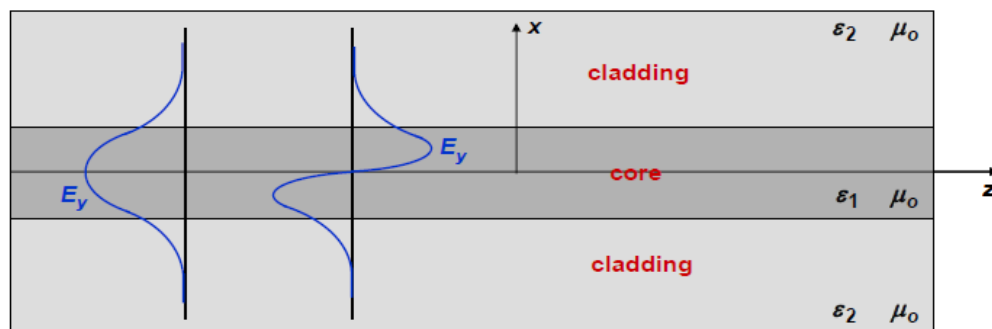

Figure 2.3: In this figure we can see the first two TE modes.

2.2   3D waveguides

In the last section we studied the slab waveguide. It is a 2D structure and it could seem useless since we live in a 3D world. However, the slab waveguide is used as a good approximation when one of the dimensions is much larger than the others.
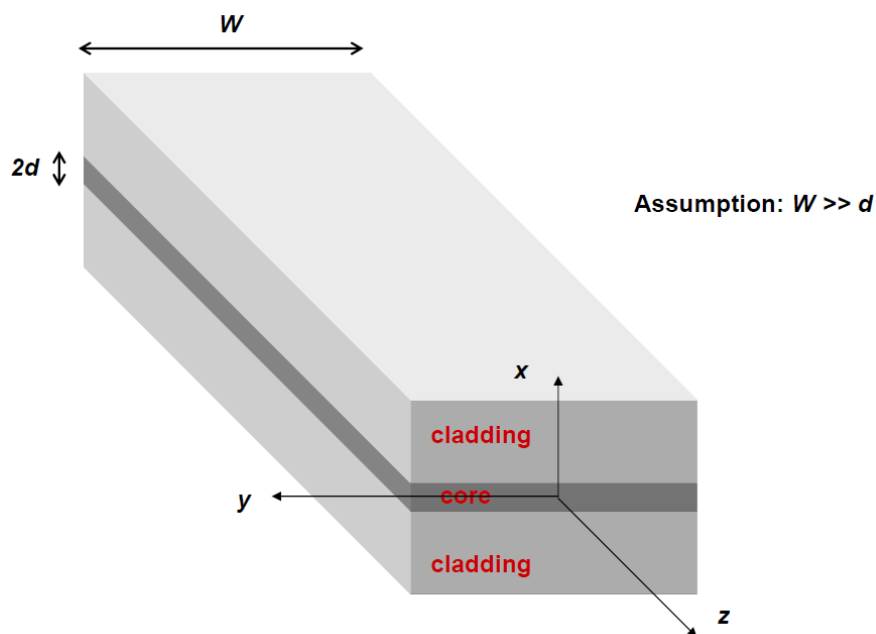
Figure 2.4: In this figure we can see the slab waveguide geometry in a three dimensional world.

When the core dimensions have the same order of magnitude in both directions at the cross section then we can not make the slab waveguide approximation. Moreover, we can not find the general expression for the modes analytically.

Figure 2.5: We can approximate the modes in x direction as a slab waveguide for the left structure. However we can not compute the y direction modes using the slab waveguide approximation. The right structure is the one we will be dealing with for our designs. It can have air cladding or SiO_2 cladding.

Therefore from now on we are going to use powerful numerical tools to deal with 3D dielectric

structures. Most of those codes have been developed by Prof. Miloš Popović during his Ph.D. and improved by the members of the group.

The first code we are going to use is the modesolver. This code gets a cross section as an input and computes the modes and propagation constants of those. It also have a visualization tool which allows to see and sort the different electric and magnetic components of the modes.
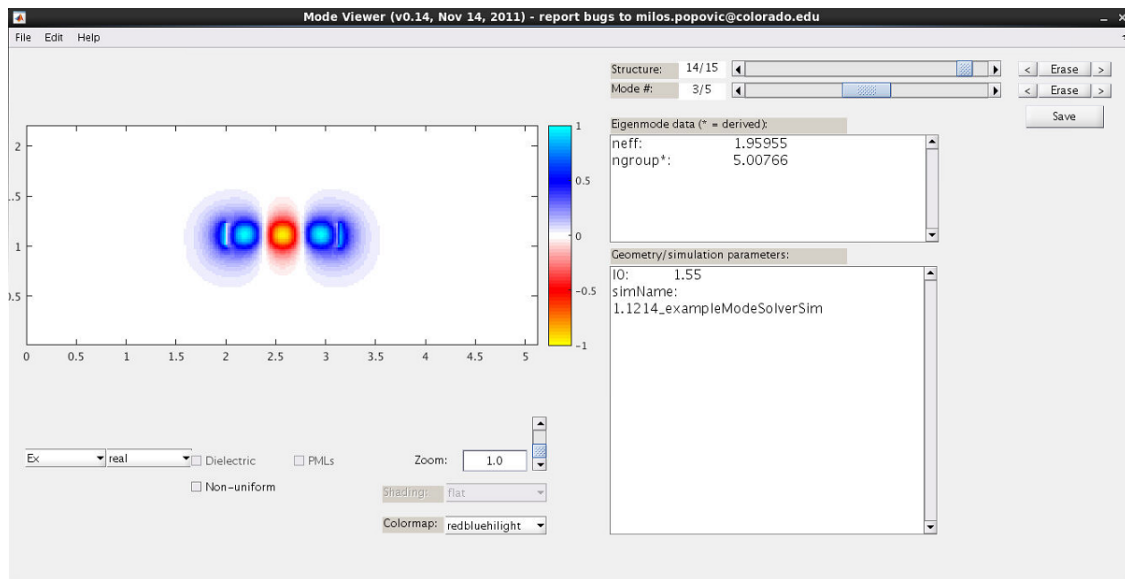

Figure 2.6: In this figure we can see the visualization tool for the mode solver. We can select the mode and the field components we want to visualize.

The first thing we can do is to visualize how the modes look like on a cross section. First we are going to show the silicon oxide structure. We will see the first three modes: TE1,TE2,TM1. We are only plotting the real part of Ex and Ey. Those components allow us to distinguish between TE and TM polarizations. TE1 has almost all the field on Ex by definition. However there is some Ey field on the edges due to edges effects. TE1 is symmetrical respect to x and y axis in component Ex and asymmetrical respect to x and y in component Ey. We can see that the TE1 mode is well confined meaning that most of the field is inside the waveguide. TM1 is the only TM mode that can be guided using a 220nm thick waveguide. We can see that is not well confined and has even

symmetry in component Ey and odd symmetry en component Ex. Finally for this width we can observe how TE2 appears. This mode is starting to be guided but if we want it to be completely guided we will need a wider waveguide. We know that a mode is guided if we can see its shape clearly on the electric field plot. An other way to see if the mode is guided is look at the dispersion plot Figure 2.9 and 2.10 This mode has one null, even parity respect to x and odd parity respect to y in component Ex.
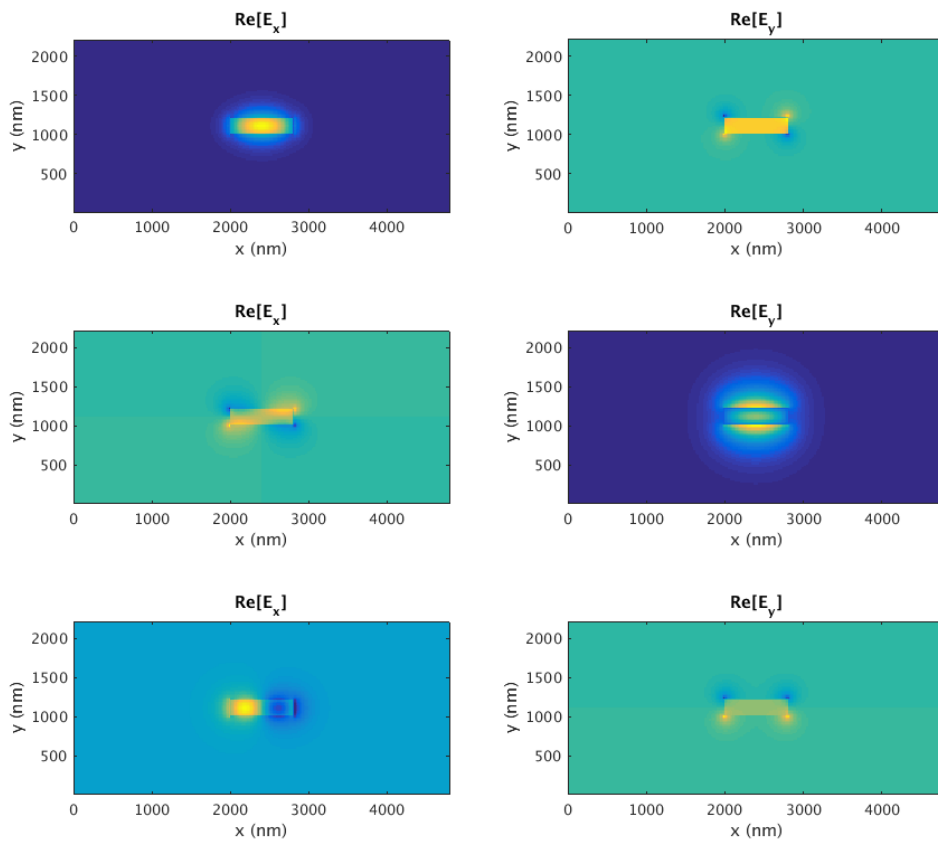

Figure 2.7: First three modes, first row TE1 second row TM1 third row TE2. 220 nm thick silicon waveguide on silicon oxide substrate and silicon oxide cladding.

Putting air as a cladding breaks the vertical symmetry. And so, the symmetry in the modes. The index contrast is higher and the modes are better confined. The propagation constants are

higher compared with silicon cladding.
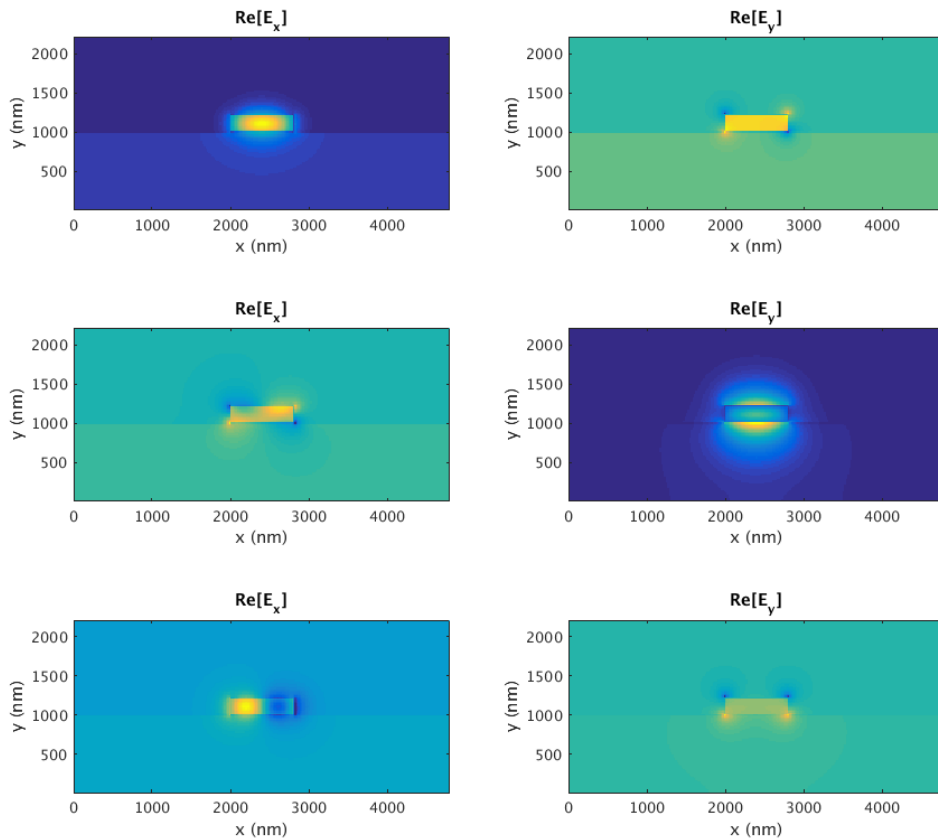
Figure 2.8: First three modes, first row TE1 second row TM1 third row TE2. 220 nm thick silicon waveguide on silicon oxide substrate and air cladding.

We have seen that the monomode cutoff for a two dimensional silicon waveguide surrounded by air is 200nm. Analogously we can compute the dispersion for air cladding and silicon oxide cladding. It is crucial for our designs to find the monomode cutoff. To avoid problems we are going to use monomode waveguides. After the simulations this results have been found:

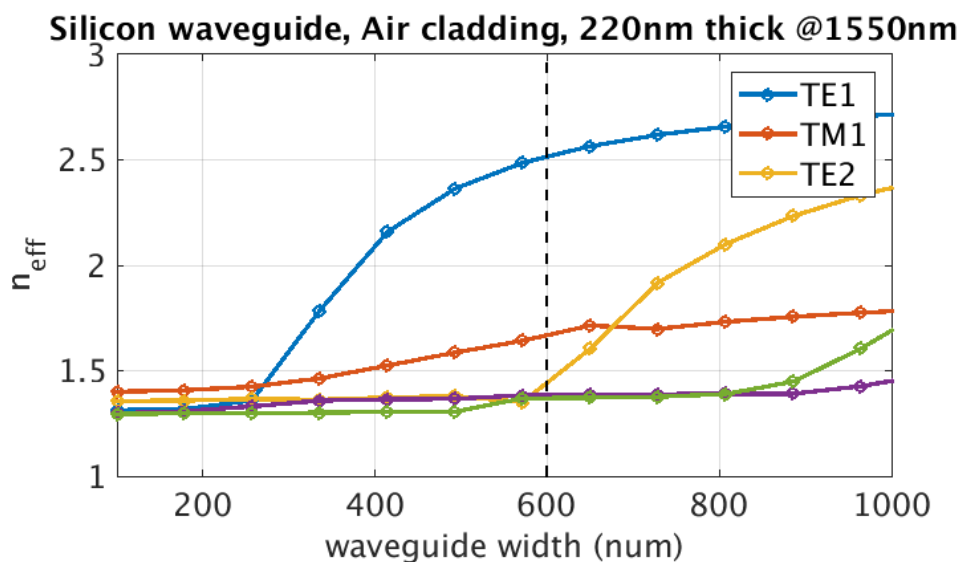| Monomode cutoff width	
SiO_2 cladding	400nm
Air cladding	600nm

Figure 2.9: Dispersion of 220 nm thick silicon waveguide on silicon oxide substrate and air cladding.
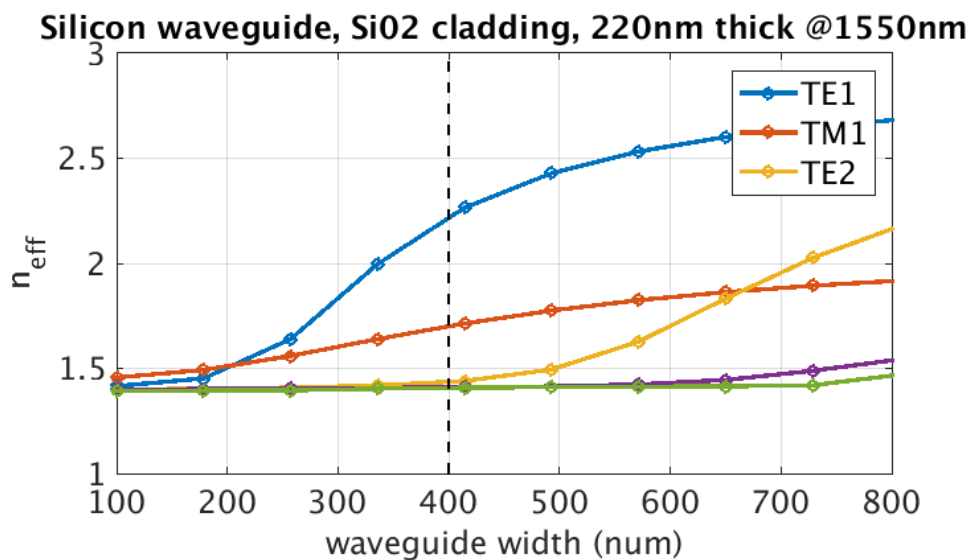

Figure 2.10: Dispersion of 220 nm thick silicon waveguide on silicon oxide substrate and silicon oxide cladding.

2.3   Coupled mode theory

In the last section we understood the single waveguide. Now we are going to see what happens when we put two waveguides close together. In order to understand that first we need to derive a mathematical theory called coupled mode theory. This theory is an approximation but it leads to pretty accurate results.

Every wave propagating though the structure can be written as a linear superposition of all the modes in that structure. Because, as we have said before, the modes are a complete set. Without losing generality, from now on we are going to focus only on TE modes. Since we are using monomode waveguides we are going to consider the fundamental TE mode only.

We start with two wave guides, they can be different. Just for fun we will pick a rectangular waveguide and a heart shaped waveguide. As we can see in the following figure each wave guide will have its own fundamental mode.
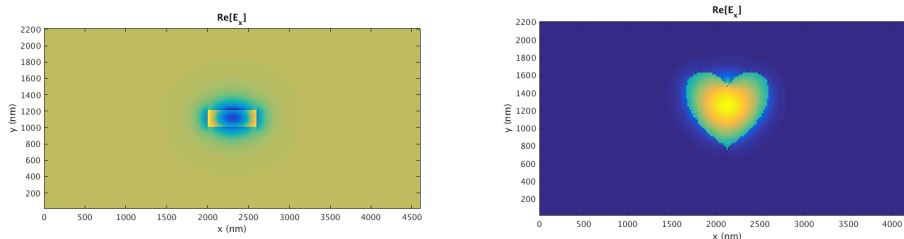

Figure 2.11: TE fundamental mode in both waveguides.

We can write the mode solution as a mode profile with a constant transversal shape propa-

gating along the waveguide as:

$$\mathbf{E}_\heartsuit = \mathbf{E}_{\mathbf{0},\heartsuit}(x,y)e^{-j\beta_\heartsuit z}$$

$$\mathbf{H}_\heartsuit = \mathbf{H}_{\mathbf{0},\heartsuit}(x,y)e^{-j\beta_\heartsuit z}$$

$$\mathbf{E}_\square = \mathbf{E}_{\mathbf{0},\square}(x,y)e^{-j\beta_\square z} \tag{2.16}$$

$$\mathbf{H}_\square = \mathbf{H}_{\mathbf{0},\square}(x,y)e^{-j\beta_\square z}$$

Now we are going to couple this modes. When two waveguides are in close proximity, they become coupled. In the following figure we can see how the modes look like when the two waveguides are close. We can observe that the modes have slightly changed in shape.
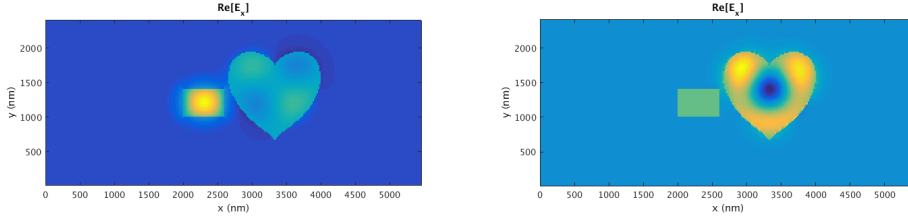
Figure 2.12: First two modes in the supermode picture.

This is called the supermode picture. This two modes considering the two waveguides are the supermodes. This modes are going to be key in the following sections.

The assumption to derive the coupled mode theory is that the supermodes can be represented as a weighted sum of the individual guided modes. This implies that the modes do not change at all with the introduction of the other waveguide. In reality, the modes are deformed slightly, but are still coupled.

$$\mathbf{E} = A(z)\mathbf{E}_\heartsuit + B(z)\mathbf{E}_\square$$

$$\mathbf{H} = A(z)\mathbf{H}_\heartsuit + B(z)\mathbf{H}_\square \tag{2.17}$$

Now we substitute these fields into Maxwell's curl equations (2.3) to obtain

$$(\hat{z} \times \mathbf{E}_\heartsuit)\frac{dA}{dz} + (\hat{z} \times \mathbf{E}_\square)\frac{dB}{dz} = 0 \tag{2.18}$$

$$(\hat{z} \times \mathbf{H}_\heartsuit)\frac{dA}{dz} - j\omega\epsilon_o(\epsilon_r - \epsilon_\heartsuit)A\mathbf{E}_\heartsuit + (\hat{z} \times \mathbf{H}_\square)\frac{dA}{dz} - j\omega\epsilon_o(\epsilon_r - \epsilon_\square)A\mathbf{E}_\square = 0 \tag{2.19}$$

We derive the generalized coupled-mode equations by substituting the above expressions into the following integral equations.

$$\int_{-\infty}^{\infty} \int_{-\infty}^{\infty} [\mathbf{E}_\heartsuit{}^* \bullet (Eq.3.18) - \mathbf{H}_\square{}^* \bullet (Eq.3.19)]dxdy = 0$$
$$\int_{-\infty}^{\infty} \int_{-\infty}^{\infty} [\mathbf{E}_\square{}^* \bullet (Eq.3.18) - \mathbf{H}_\heartsuit{}^* \bullet (Eq.3.18)]dxdy = 0 \tag{2.20}$$

After lots of algebra, we get the generalized coupled-mode equations. These are solved to describe the coupling between the two waveguides.

$$\frac{dA}{dz} + c_{\heartsuit\square}\frac{dB}{dz}e^{-j(\beta_\square-\beta_\heartsuit)z} + j\chi_\heartsuit A + j\kappa_{\heartsuit\square}Be^{-j(\beta_\square-\beta_\heartsuit)z} = 0$$
$$\frac{dB}{dz} + c_{\square\heartsuit}\frac{dA}{dz}e^{-j(\beta_\square-\beta_\heartsuit)z} + j\chi_\square B + j\kappa_{\square\heartsuit}Ae^{-j(\beta_\square-\beta_\heartsuit)z} = 0 \tag{2.21}$$

Where $\kappa_{\heartsuit\square}$ is the mode coupling coefficient

$$\kappa_{\heartsuit\square} = \frac{\omega\epsilon_o \int_{-\infty}^{\infty} \int_{-\infty}^{\infty} (\epsilon_r - \epsilon_\square)\mathbf{E}_\heartsuit{}^* \bullet \mathbf{E}_\square dxdy}{\int_{-\infty}^{\infty} \int_{-\infty}^{\infty} \hat{z} \bullet (\mathbf{E}_\heartsuit{}^* \times \mathbf{H}_\heartsuit + \mathbf{E}_\heartsuit \times \mathbf{H}_\heartsuit{}^*)dxdy} \tag{2.22}$$

$c_{\heartsuit\square}$ is the butt coupling coefficient

$$c_{\heartsuit\square} = \frac{\int_{-\infty}^{\infty} \int_{-\infty}^{\infty} \hat{z} \bullet (\mathbf{E}_\heartsuit{}^* \times \mathbf{H}_\square + \mathbf{E}_\square \times \mathbf{H}_\heartsuit{}^*)dxdy}{\int_{-\infty}^{\infty} \int_{-\infty}^{\infty} \hat{z} \bullet (\mathbf{E}_\heartsuit{}^* \times \mathbf{H}_\heartsuit + \mathbf{E}_\heartsuit \times \mathbf{H}_\heartsuit{}^*)dxdy} \tag{2.23}$$

$\chi_\heartsuit$ is the change in propagation constant

$$\chi_\heartsuit = \frac{\omega\epsilon_o \int_{-\infty}^{\infty} \int_{-\infty}^{\infty} (\epsilon_r - \epsilon_\square)\mathbf{E}_\heartsuit{}^* \bullet \mathbf{E}_\heartsuit dxdy}{\int_{-\infty}^{\infty} \int_{-\infty}^{\infty} \hat{z} \bullet (\mathbf{E}_\heartsuit{}^* \times \mathbf{H}_\heartsuit + \mathbf{E}_\heartsuit \times \mathbf{H}_\heartsuit{}^*)dxdy} \tag{2.24}$$

$\chi_\square$ will be the same expression (2.24) but changing hearts to squares.

Where ϵ_r is the dielectric function containing both waveguides and $\epsilon_\square$ is the dielectric with only $\square$ waveguide.

The most important coefficient is the coupling coefficient. This parameter quantifies how efficiently power leaks from waveguide $\heartsuit$ to waveguide $\square$ due to the behavior of the supermode. If we change $\heartsuit$ for $\square$ and $\square$ for $\heartsuit$. We will get a coupling coefficient that tells how efficiently power leaks from $\square$ to $\heartsuit$.

The coefficient $c_{\heartsuit\square}$ quantifies the excitation efficiency from one waveguide to an other. If the waveguides are sufficient separated then $c_{\heartsuit\square} \approx 0$ and $\kappa_{\heartsuit\square} \approx 0$.

Finally the coefficient $\chi_\heartsuit$ measure how the propagation constant of $\heartsuit$ changes due to the fact that $\square$ is close. This coefficient increases as the gap between waveguides is smaller. Normally we will neglect this term because is much lower than the other two.

We know that the total power in wave guide $\heartsuit$ is

$$P_\heartsuit = \frac{1}{2} \int_{-\infty}^{\infty} \int_{-\infty}^{\infty} [\mathbf{E}_\heartsuit \times \mathbf{H}_\heartsuit^*] \bullet \hat{z} dx dy \tag{2.25}$$

The observe that the denominator in all the coefficients is equal to $4P_\heartsuit$. Without losing generality we will normalize the power according to $4P_\heartsuit = 1$. Then can be shown that $c_{\heartsuit\square} = c_{\square\heartsuit}^*$ and $\chi_\heartsuit = \chi_\square^*$.

If we substitute the fields on equation (3.25) and we work the algebra we will find the following expression for the power:

$$P = \frac{1}{4}[| A |^2 + | B |^2 + A^* B c_{\heartsuit\square} e^{-j2\delta z} + A B^* c_{\square\heartsuit}^* e^{j2\delta z}] \tag{2.26}$$

where $\delta = \frac{\beta_\square - \beta_\heartsuit}{2}$. Assuming that the waveguides are loss-less the power has to be conserved and

so

$$\frac{dP}{dz} = 0 \tag{2.27}$$

$$jA^*B(\kappa^*_{\square\heartsuit} - \kappa_{\heartsuit\square} - 2\delta c\heartsuit\square)e^{-j2\delta z} - jAB^*(\kappa_{\square\heartsuit} - \kappa^*_{\heartsuit\square} - 2\delta c\heartsuit\square)^* e^{-j2\delta z} = 0 \tag{2.28}$$

And this has to be satisfied for all z, then we must have $\kappa_{\square\heartsuit} = \kappa^*_{\heartsuit\square} + 2\delta c^*_{\heartsuit\square}$. Then if the waveguides are similar and not super close then $\kappa_{\square\heartsuit} = \kappa^*_{\heartsuit\square}$. In our heart shape waveguide example we could not be able to neglect $c_{\heartsuit\square}$ but since we are going to use square similar waveguides we can assume $c_{\heartsuit\square} = \chi_\heartsuit = 0$. Finally we found the coupled-mode equations.

$$\frac{dA}{dz} = -j\kappa_{\heartsuit\square}Be^{-j(\beta_\square - \beta_\heartsuit)z}$$
$$\frac{dB}{dz} = -j\kappa_{\square\heartsuit}Ae^{-j(\beta_\square - \beta_\heartsuit)z} \tag{2.29}$$

This simple equations describe how the power bounces around from one mode to an other [8].

Chapter 3

Types of 2x2 power couplers

In this chapter we will present and compare the main three 2x2 couplers on the literature: direcitonal couplers, adiabatic couplers and MMIs.

3.1 Directional Coupler

In the last section we have derived the basic equations of coupling mode theory. We also introduced key concepts such as the coupling coefficient. Now we have the tools to study the directional coupler. First we are going to approach the directional coupler analytically using coupled mode theory and finally we are going to use finite differences in time domain to solve the problem numerically.

3.1.1 Directional Coupler: CMT approach

A directional coupler consist of two parallel waveguides [6]. Those waveguides are separated by a gap g. They have width $w1,w2$ which does not change along z. And they can have air or silicon oxide cladding with a thickness t.
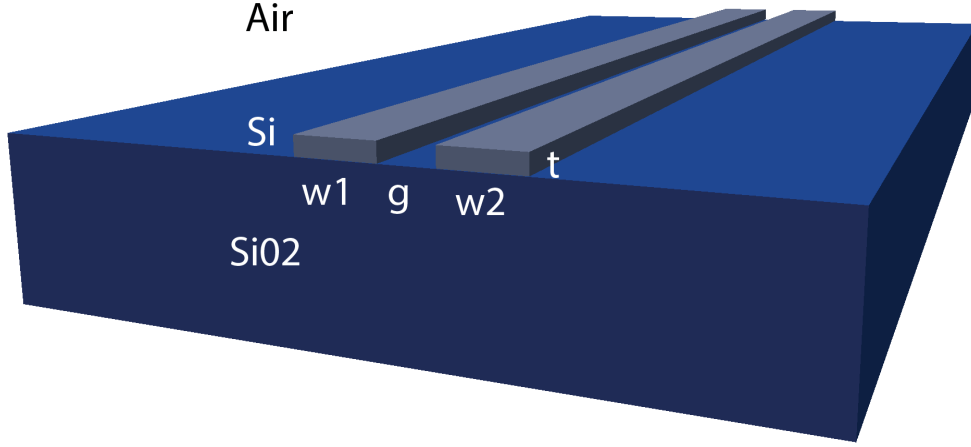
Figure 3.1: Directional coupler geometry.

We start pumping light in one of the wave guides. Therefore the initial conditions to solve equation 2.29 will be $A(0) = A_0$ and $B(0) = 0$. Therefore is trivial to get the solutions for the evolution of the amplitudes along the directional coupler.

$$A(z) = A_o[cos(\psi z) + \frac{j\delta}{\psi} sin(\psi z)]e^{-j\delta z}$$

$$B(z) = -A_o \frac{j\kappa}{\psi} sin(\psi z)e^{j\delta z}$$

$$(3.1)$$

where $\kappa = \kappa_{AB} = \kappa_{BA}^*$, $\delta = \beta_A - \beta_B$ and $\psi = \sqrt{\kappa^2 + \delta^2}$.

It makes more sense to express the last expression in terms of power instead of amplitudes.

$$P_A(z) = \frac{\mid A(z) \mid^2}{\mid A_o \mid^2} = 1 - Fsin^2(\psi z)$$

$$P_B(z) = \frac{\mid B(z) \mid^2}{\mid B_o \mid^2} = Fsin^2(\psi z)$$

$$(3.2)$$

Where F is the maximum power-coupling efficiency

$$F = \frac{\kappa^2}{\psi^2} = \frac{1}{1 + \frac{\delta^2}{\kappa^2}}$$

$$(3.3)$$

From the expression for power-coupling efficiency we can deduce that we will only be able to transfer all the power form one waveguide to the other if $\frac{\delta}{\kappa} = 0$. This can happen if $\kappa \ggg \delta$, i.e. waveguies with similar sizes and close together. However if the waveguides get closer and closer then the approximations we have done are less valid. The other way to be able to achieve 100% power transfer is using the same exact width for both waveguides.
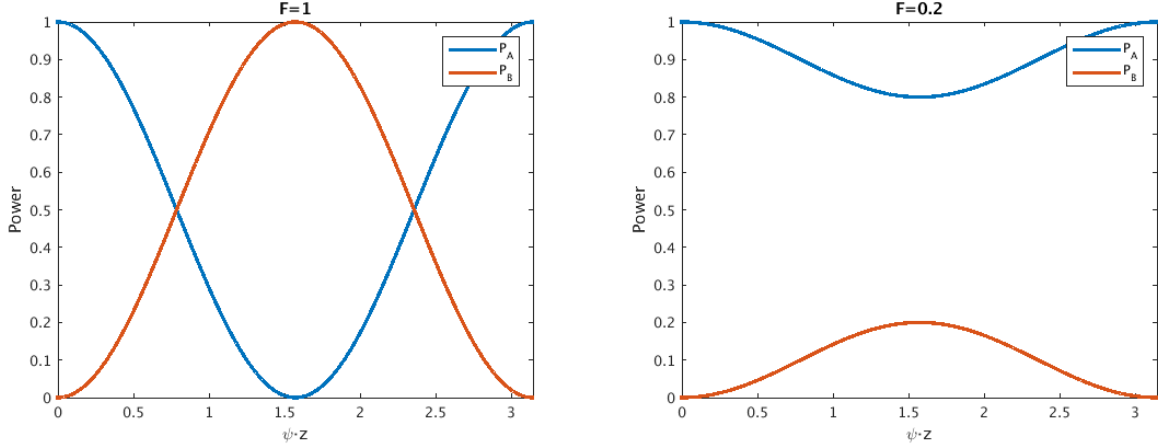

Figure 3.2: Power in each mode vs z

The aim of this section is to design a directional coupler. So we would want an even power at the outputs for a single port input. In order to do that we will look for the length L_{3dB} where we have 50-50 power transfer.

$$L_{3dB} = \frac{1}{\psi} asin(\frac{1}{\sqrt{2F}}) = \frac{asin(\sqrt{\frac{1+(\frac{\delta}{\kappa})^2}{2}})}{\sqrt{\kappa^2 + \delta^2}} \tag{3.4}$$

This equation has solution if $F > 0.5$ otherwise we can not achieve 50% transmission form the first waveguide to the second. This condition leads to a condition for δ and κ.

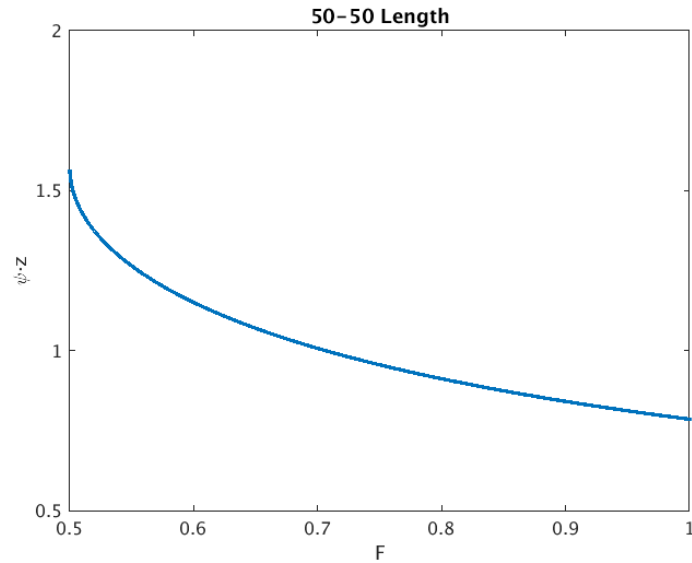$$\delta \leqq | \kappa | \tag{3.5}$$

Figure 3.3: Plotting equation 3.4 $L_{3dB}\psi$-F

If $F = 1$ we have a directional coupler. For $F < 1$ we have a delta-beta coupler. For the case where $F = 0.5$ we do not need exactly L_{3dB}. We can tolerate some variations on L_{3dB} and still have 50-50 splitting because the design is first order invariant with length. That can be seen in Figure 3.2.
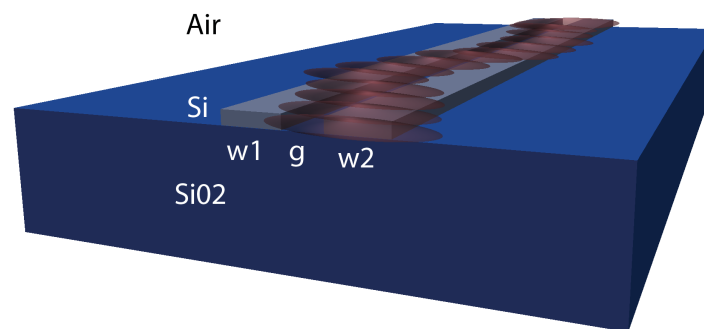

Figure 3.4: Artistic representation of our directional coupler. We start with all the power in one wavguide then it starts bouncing form one waveguide to the other. Every period we can find a length which splits the power evenly.

3.1.2   Directional Coupler: FDTD approach

We have seen the theory behind the directional coupler. One of the best ways to simulate the propagation of electromagnetic waves through dielectrics is finite differences time domain, or FDTD. There are some commercial software that are able to do FDTD simulations. However we have been using the code wrote by Christina Manolatou. She wrote most of the fortran code, my advisor Miloš Popović made some smaller additions and wrote matlab postprocessing, then people in our group built the matlab input interface.

For every simulation we have to define the structure in a three dimensional matrix, the positions of the sources and the position for the observation plains. The code can work in 2D supposing one dimension infinite (i.e. slab waveguides) or 3D. We did the study considering 2D just because the simulations took less time. We will skip the 3D results and we will see directly the results in 2D.

The aim is simulating low-loss couplers. To do that we want to avoid something called numerical scattering. The numerical scattering is caused due to the discritization. If the discritization is small enough we will not have numerical scattering. However, the minimum discritization that we can use to solve the structure in a reasonable time is $dx = 10nm$. In order to solve that problem we will use a Fermi-Dirac distribution to smooth the edges.

There is no specific reason to use a Fermi-Dirac distribution instead of other function besides it works. When I arrived at the lab they were already using this technique to reduce the numerical scattering.
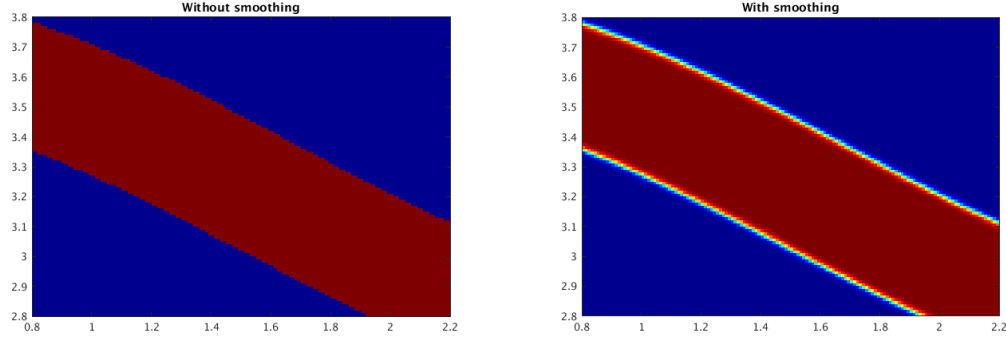
Figure 3.5: On the left: waveguide without smoothing. On the right: smoothed waveguide

The Fermi-Dirac equation we are using to smooth the edges is

$$y = \frac{1}{1 + ln(9)e^{\frac{ax}{1.5dy}}} \tag{3.6}$$

where a is a parameter that controls how many pixels are going to be smoothed. The smoothing should be performed perpendicular to the curve at each point. However, we apply the smoothing in y direction since is the mostly affected direction due to discretization.
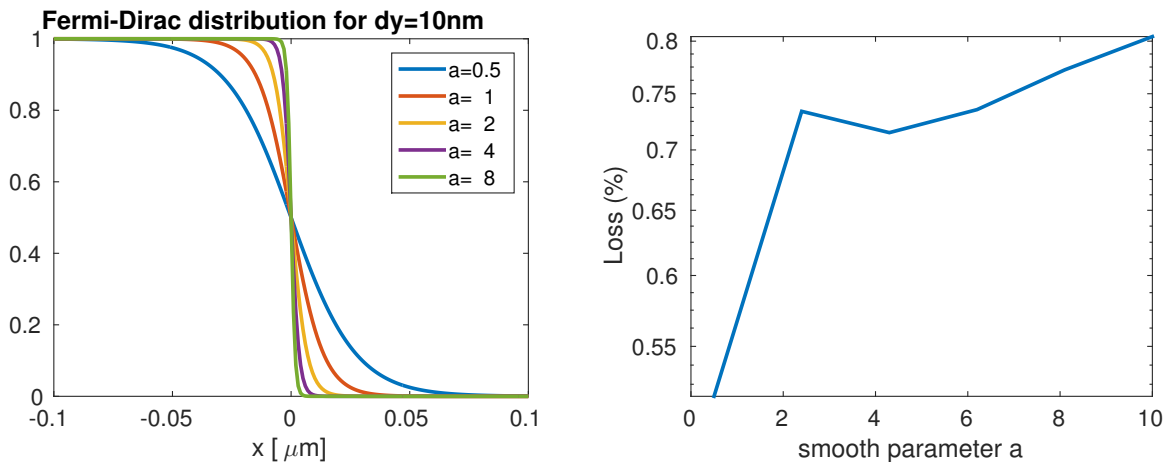

Figure 3.6: On the left: Fermi-Dirac distribution for different values of a. On the right: Loss on the structure versus the smooth parameter a.

We want to see the effect of the smooth parameter on the dielectric. We have simulated a sinusoidal bend using the FDTD code. We keep track of the losses on the structure while changing the parameter a. For now on we are going to chose a value of $a = 1$ since give us low loss.

In order to simulate the directional coupler we will add a bending input and bending output. This sinusoidal bends will couple some light when we get closer to the coupling region. Therefore we have to modify the coupling equation in order to take into account this extra coupling due to the bend region. Then we will have the cross port power K^2 and the through port power T^2.

$$K^2 = sin(\frac{\pi}{2L_z}[L + z_{bend}])^2$$

$$T^2 = cos(\frac{\pi}{2L_z}[L + z_{bend}])^2$$

(3.7)

Where L_z is the cross-over length and z_{bend} represents the effective extra coupler distance introduced by the coupling from the non-parallel waveguides.
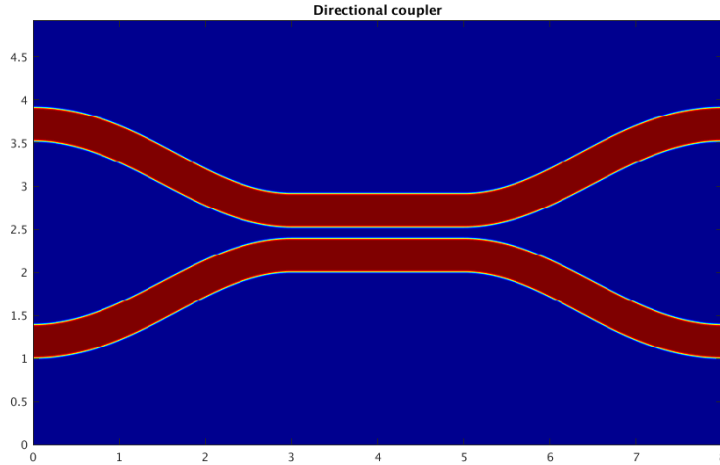

Figure 3.7: Directional coupler dielectric.

Now we can simulate the directional coupler for different coupling lengths and fit the curve to the theoretical equation. And thus we can find L_z, z_{bend}. We will chose air cladding and 160nm width for both waveguides.

Once we found the desired length to make the device work as a beamsplitter we can look at its dependence with wavelength. As we can see in the figure the transmission coefficients highly depend on wavelength. So, the directional coupler can be a short beamsplitter but not a broadband.
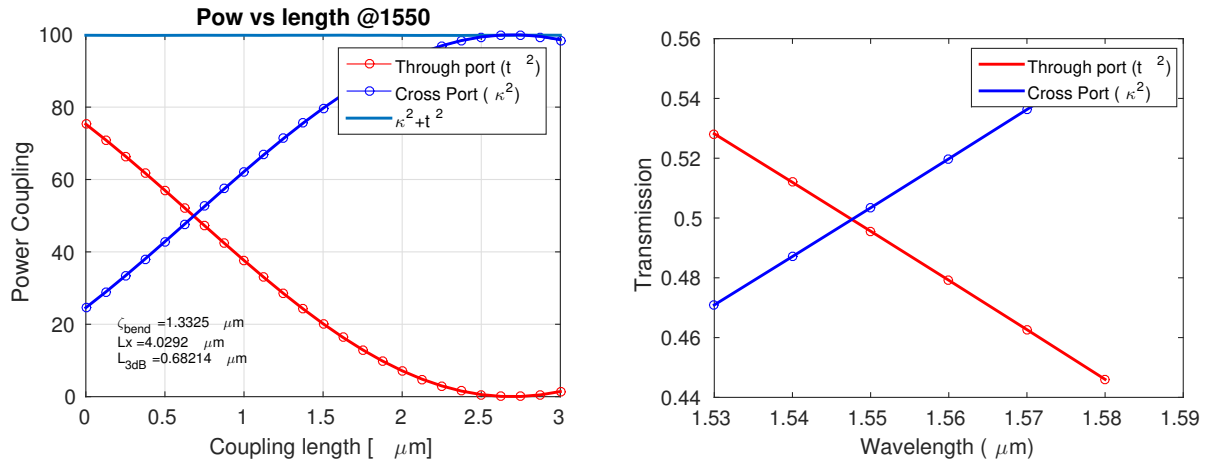

Figure 3.8: On the left: Directional coupler, power versus length. On the right: Directional coupler, power versus wavelength at 50-50 length condition.

A variation of the directional coupler is the delta-beta directional coupler [5]. As we have seen before if we make the waveguides width different then we can not achieve 100% power transfer from one waveguide to the other one. So the cross port power transfer will be.

$$K^2 = \frac{sin^2(\kappa L\sqrt{1 + (\frac{\triangle\beta}{2\kappa})^2}}{1 + (\frac{\triangle\beta}{2\kappa})^2} \tag{3.8}$$
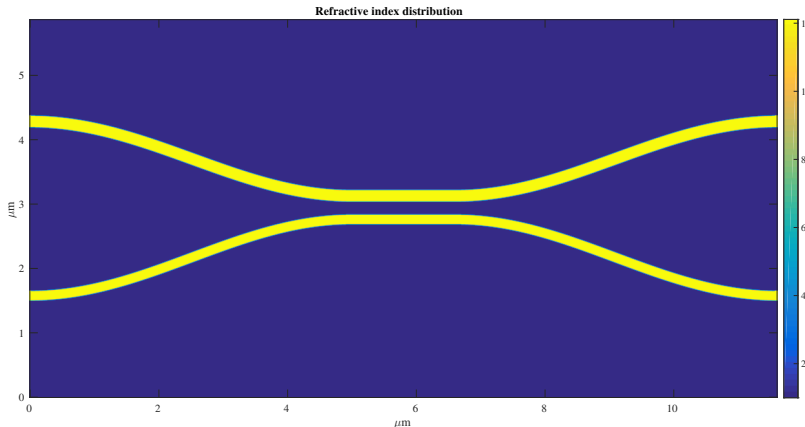
Figure 3.9: Delta-Beta Directional coupler dielectric.

Using this principle we can find the width that make exactly 50% power transfer at maximum. As we saw in the last section. In this way we can design a first order invariant structure with respect to coupling length. We chose air cladding and 180 and 150 nm width. So we chose length $1.6\mu m$ and we can see that as the directional coupler is highly dependent on wavelength.
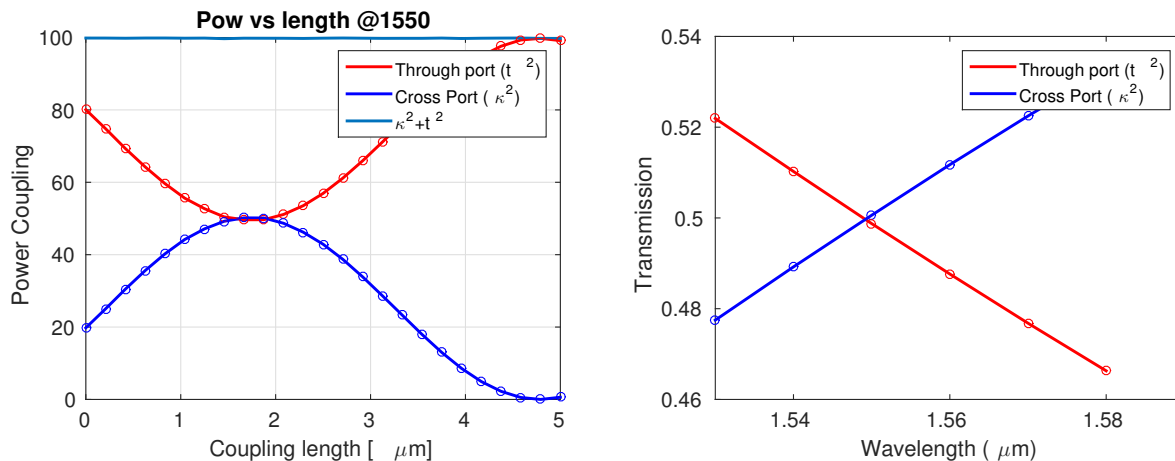

Figure 3.10: On the left: Delta-Beta directional coupler, power versus length. On the right: Delta-Beta directional coupler: power versus wavelength at 50-50 length.

3.2   Adiabatic coupler

So far we have talked about z invariant structures. In those structures the waveguide width does not change along the propagation direction. In this section we are going to explore what happen when the geometry change in z direction. We will use those results to design an another kind of coupler, the adiabatic coupler [9].

We have already talked about the orthogonality condition in modes. This condition can not be satisfied in waveguide structures in which the waveguide parameters vary in the direction of propagation. It can not be satisfied in the sense that we can not find the same base of orthogonal modes at each cross section along z. However we can define the local normal modes at the position z_0. The local normal mode representation will now become a function of z.
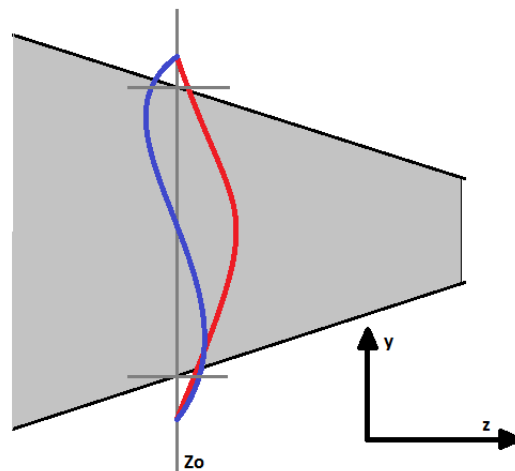
Figure 3.11: To define a local normal mode, the slowly varying waveguide structure (darker line) is replaced at z_0 by the structure of constant with z (less darker line), and the normal mode solutions at z_0 are obtained.

The amplitudes of the local normal modes along the structure can vary in contrast to the fixed structure. Power transfer between the local normal modes of a varying structure will occur, and we will see the power transfer depends on the change of rate on the geometry.

We have to modify the coupled mode theory due to the variation in z. We are not going to derive the equations but a rigorous derivation can be found on [2]. The main idea to find the equations is write the mode of each local slice in terms of the modes of the slice right before. In this way we can find power transmission from z to $z + dz$. For the forward modes.

$$\frac{\partial A_i}{\partial z} = -C_{ij}A_j + j\beta_i A_i \tag{3.9}$$

where the subscripts i and j refer to the fundamental and next higher order systems modes. Here $(Ai, Aj),(\beta_i, \beta_j)$ and C_{ij} are the corresponding amplitudes, propagation constants, and normalized coupling coefficient between these modes. The expression for the coupling coefficient can be found on [10].

$$C_{ij} = \frac{k_0}{4}\sqrt{\frac{\epsilon_0}{\mu_0}}\frac{1}{\Delta\beta_{ij}}\int_A \hat{e}_i^* \cdot \hat{e}_j \frac{\partial n(x,y)^2}{\partial z}dA \tag{3.10}$$

We define a slow or adiabatic waveguide transition as a transition between two waveguide structures that takes place so slowly that negligible power transfer occurs between the normal modes. That happen when the rate of change of the walls is small in z direction. Then $\frac{\partial n(x,y)^2}{\partial z} \longrightarrow 0$ and no interaction appears between different modes.

$$\frac{\partial A_i}{\partial z} = j\beta_i A_i$$
$$\frac{\partial A_j}{\partial z} = j\beta_j A_j \tag{3.11}$$

This happen if $\delta \gg \kappa$. Then we can lunch the first mode A_1 of the structure at $z = 0$ and

ideally the power in the second mode A_2 at length L will be

$$\frac{\mid A_2(L) \mid^2}{\mid A(0) \mid^2} \longrightarrow 0 \tag{3.12}$$

This means that all the power will remind in the first mode. Notice that at each slice the modes are changing. By adiabatic assumption the geometry will change slowly. However for a long structure we can start in one geometry and end in a completely different one. This is the key concept to design a low loss broad-band coupler.

We will start with two waveguides separated in order to not have coupling at all between them. We want the width of this two waveguides to be different. In this way the two first supermodes will have different propagation constants. The first mode will correspond to the wider waveguide. We want to change this cross section with a large gap and two waveguides with different width to a cross section with a small gap and two equal waveguides. The modes in this last section will be the symmetrical and the antisymmetrical. If our structure is long enough to be adiabatic then the first mode at the beginning will lead to the first mode at the end. And the same for the second mode.
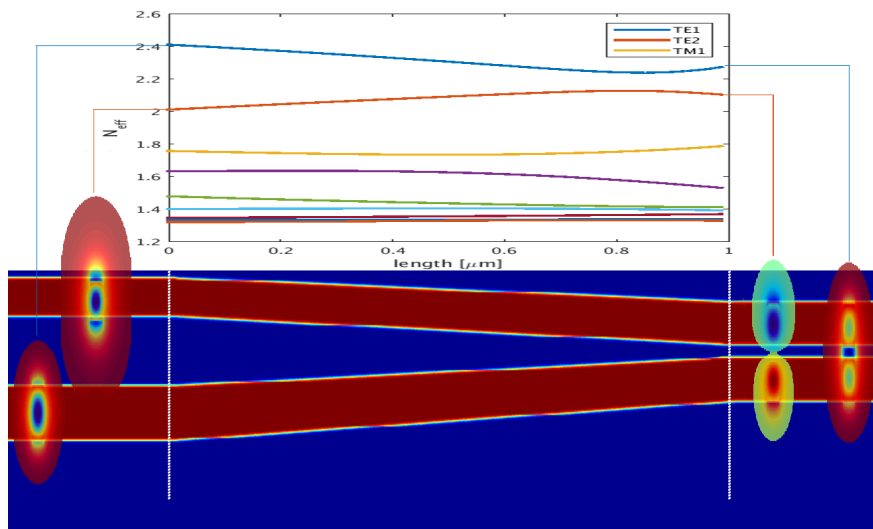

Figure 3.12: We can see how the structure is and which are the modes at the first and last section. We can also see how the propagation constant evolve with z.

If we have two equal waveguides at the last slice and we have all the power in ether the first mode or the second mode. Then we have half of the power in each wave guide. Then we need to separate the two waveguides apart to have two different outputs. If we do that in a symmetrical way no power will transfer from one waveguide to the other.

Despite this structures are robust,broadband and easy to design they tent to be really long ($\sim$ $100\mu m$). This is not a problem if we do not care about space, but if we want to package a 2x2 couplers network we may have to use an other kind of coupler.

We can not use FDTD to simulate those structures because they are too long. So, in order to simulate them we are going to use a film mode matching code (FMM), written by Prof. Miloš Popović.

We are going to simulate only the adiabatic region. We are going to keep tracking of the power for each symmetrical and antisymmetrical mode. Ideally we want to pick the length that makes the power on the antisymmetrical mode zero. But for a real design we need the minimum length that makes the device work under some conditions. We impose the minimum error ratio has to be 1% in power, so 49-51% ratio. This means having less than 1e-4 of the normalized power in the antisymmetrical mode.
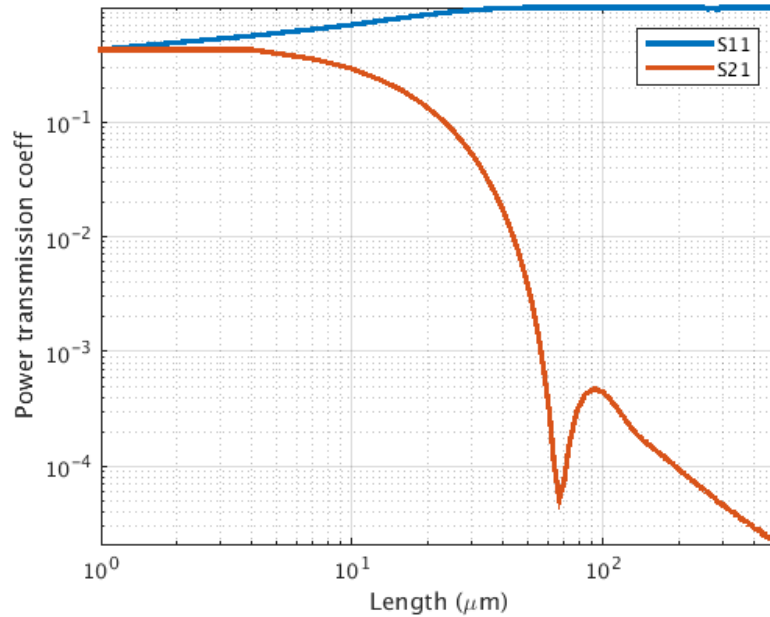
Figure 3.13: Observation plain: last section where the two waveguides are the same width. We can see the rate of power for the symmetrical mode and the antisymmetrical vs device lengths.

From the plot we can see that at length near to $70\mu m$ the device could work. However this length is really sensitive, a little change on length is going to change a lot the fraction of power in the antisymmetrical mode. In order to avoid that we would pick a length higher than $200\mu m$ which is really long.

3.3   Summary

We have seen in the last few sections the directional coupler and the adiabatic coupler. The other promising coupler is the multimode interference coupler (MMI) proposed on [1]. We simulated the first two because the main concepts that make them work are useful to understand the new coupler we will present in the next chapter. So simulating or explaining the MMI is out of the scope of this thesis. However we will compare our new coupler with the best three 2x2 types of couplers in the literature.

The directional coupler can be really short $\backsim$ $5\mu m$ and low loss but is highly wavelength dependent. In opposition to the adiabatic coupler which is really long $\backsim$ $200\mu m$ and low loss but is really broadband. On [4] the authors compare a directional coupler and optimize an adiabatic coupler. The results they got are pretty impressive. They use a silicon ridge waveguide with 150nm thickness for each etching. Their adiabatic coupler is $150\mu m$ on the coupling region but taking in to account the waveguides from the gradings in and out the footprint is $650\mu m \times 150\mu m$. They used and optimized the design proposed on [12]. On simulations they got: power ratio of $\backsim$ 0.00521dB over 60nm (1271-1331nm). They show that with a fabrication error of 10nm on the waveguide width the power ratio goes to 0.05dB. The MMI gets a good trade off on shortness, broadband and fabrication errors tolerance. The best MMI in the literature so far on the 220nm silicon thick platform gives a simulated: power ratio of $\backsim$0.1dB, insertion loss $\backsim$0.11dB over 36nm (1530nm-1566nm). This device has a food print of $3.8\mu m \times 152\mu m$. The tapers in are 50 [3].

Even though we can not compare apples with apples since the adiabatic coupler has not a 220nm silicon layer cross section. The recent results give us an idea of how good the performance on adiabatic couples can be. The results on the MMI are pretty promising too.

Chapter 4

Frustrated coupling based adiabatic coupler

4.1 Frustrated coupling based adiabatic coupler

4.1.1 The concept

We have seen the three main 2x2 coupler strategies on the literature. In this section we are going to propose a new type of 2x2 coupler. This new type of coupler its called frustrated coupling based adiabatic coupler and it will be really short, low-loss and broadband. In order to do that we are going to use concepts from both directional and adiabatic coupler and we are going to create and hybrid. The key idea to this design came from my advisor Prof. Miloš Popović when he was doing his Ph.D. at MIT back in 2005. One day he was trying his FMM code, he was simulating the same kind of adabatic couplers like the ones we saw in the last section. He was trying to tilt that structure. He realized that the coupling from one layer the the next one changes with tilting. But even more, changing the tilting direction changes the sign of the coupling coefficient. Which means that exist a tilt of the structure that makes the coupling from the first to the second mode zero. So now instead of trying to change slowly the structure to avoid coupling what we will do is to make the whole integral from Eq. 3.10 equal to zero by bending the structure.
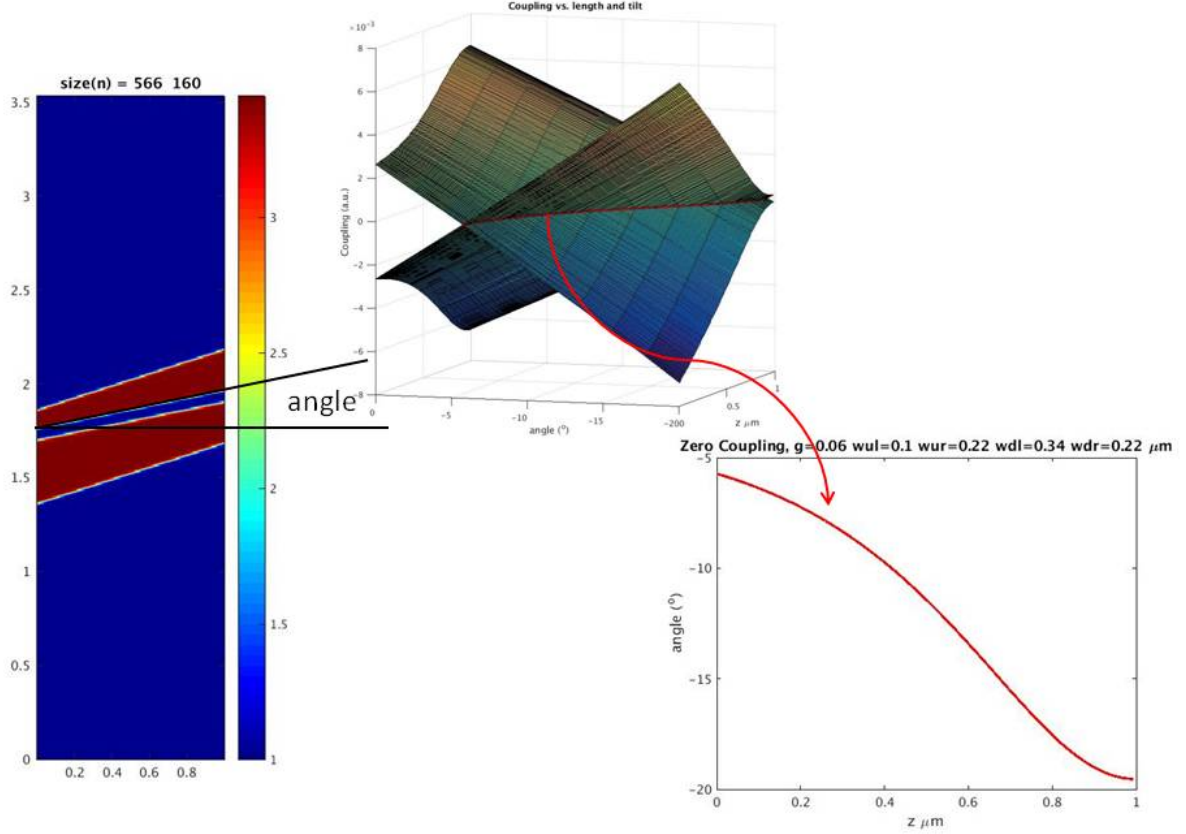
Figure 4.1: On the left we have the top view of the dielectric. We change the angle and compute the coupling coefficient κ_{12} and κ_{21} at each angle and across the propagation direction. On the middle section we plot κ_{12} and κ_{21} vs z and angle. On the right we plot the intersection at zero coupling of κ_{12} and κ_{21} vs angle and z.

The design will consist on the following geometry. Analogously to the adiabatic coupler. We start with a wide waveguide and a thin one. In this way we can separate the propagation constant from the first and second mode. Then keeping the gap constant we go from different width to the same width. We do this transition linearly.

$$w^i(z) = \frac{w^i_{final} - w^i_{initial}}{L} z + w^i_{initial} \tag{4.1}$$

For i=1,2. And thus on the last cross section the light will be split equally between waveguides.

First we have to chose the parameters for $w^1(0), w^1(L), w^2(0), w^2(L)$ and g. The number of degrees of freedom is 3 for the first section and 2 for the last section. We are going to simulate the first and last section and see how the geometry change the effective index of the three first modes. In order to help this process we not only want to avoid coupling from the first to the second mode but also from the second to the third. The condition then is to find the geometry that give us the maximum distance from N_{eff1}, N_{eff2} and N_{eff2}, N_{eff3}. This means that $N_{eff2} - N_{eff1} \approx N_{eff3} - N_{eff2}$. Where N_{effj} is the effective index for the jth TE mode.

We are going to use silicon cladding structures for the 3D simulations. The reason for that is to simplify the problem. Having a horizontal symmetry on the cross section avoid coupling from TE to TM modes. Then we only have to worry about TE modes.

We will start with the last section since it is easier. After simulating the cross section we realized that roughly as small the gap the better. Then we pick a $g = 100nm$ since is the smallest gap we can fabricate without any problems. Then we consider which width to pick. We know that $w^1(L) = w^2(L)$ to have the symmetrical mode in the last section. After plotting the effective index for the three first modes we decided that the best width is $w(L) = 380nm$. Then by trial and error we find that the best width are $w^1(0) = 480nm$ and $w^2(0) = 340nm$.
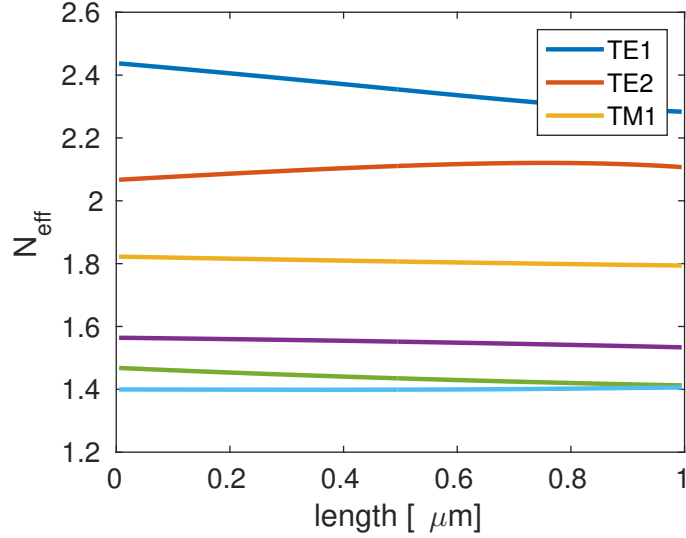
Figure 4.2: Neff versus normalized length for the following geometry: $w1(0) = 480nm$, $w2(0) = 340nm$, $w(L) = 380nm$, $g = 100nm$. Notice that the N_{eff} does not depend on the tilting.

We found two ways to generate the structure. The first one is to use the information obtained on Figure 4.1. Since the information on the right plot is local, we can integrate the angles to generate the desired structure. The other way to generate the structure is more automatized. We start the algorithm to design the structure with only the first cross section. We compute the modes on this section with the FMM code. Then we introduce a new slice. The widths on this slice will be slightly different since we moved a step in z direction. Then we are going to slide this layer in x direction an amount ρ. If we do that for positive and negative values of ρ and we plot κ_{12} and κ_{21} we will see that there is a sweet spot where they go to zero.
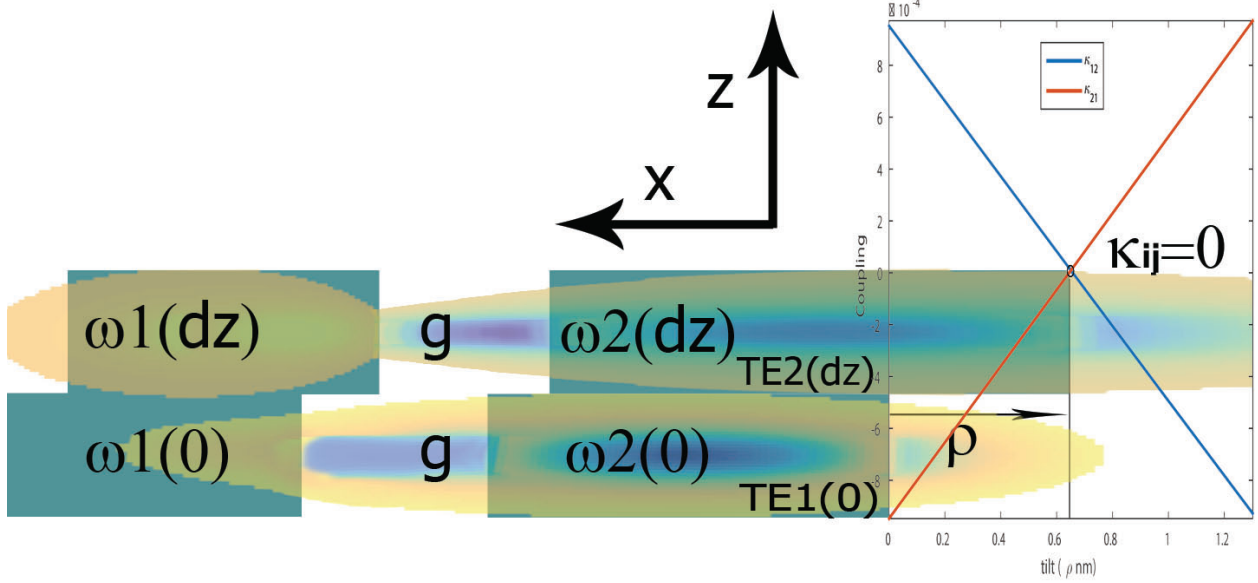
Figure 4.3: This figure is key to understand this last section. We can see on the background the two first slides of our design. Both layers have different width because the widths change with z. We are showing the first mode on the first section and the second mode on the second section. The overlap integral between those two modes and a term considering the variation on the dielectric from section one to section two gives us κ_{12} (Eq. 3.10). Then we can move the second slice an amount ρ to the right. There is a ρ_0 where the $\kappa_{12} = \kappa_{21} \approx 0$

Notice that the coupling in one slice only depends on the layer right before. We can repeat this process until the last section. After doing that we will have a structure that avoids coupling from one supermode to the other.
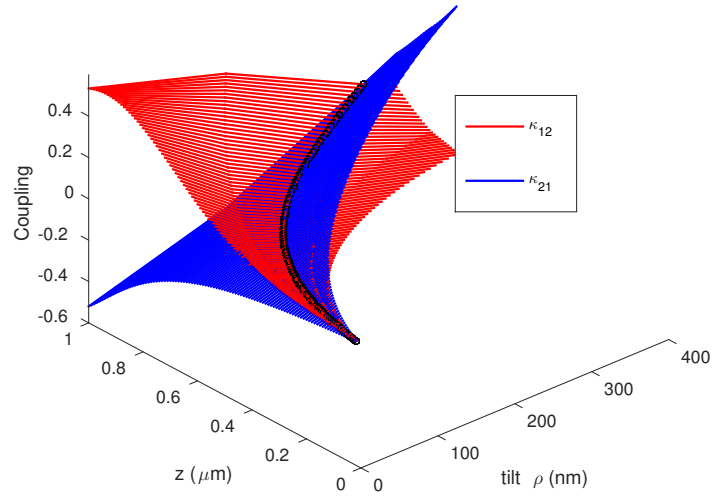
Figure 4.4: Coupling coefficients κ_{12} and κ_{21} versus tilt versus z. We can find the zero coupling condition for each z_0 $(\rho_0(z_0))$.

Once we have $\rho_0(z)$ we can simulate the structure performance using the FMM code. As we can see, even though we found the intersection for the two surfaces κ_{12} and κ_{21}, that condition does no lead to zero coupling. However it minimizes the coupling.
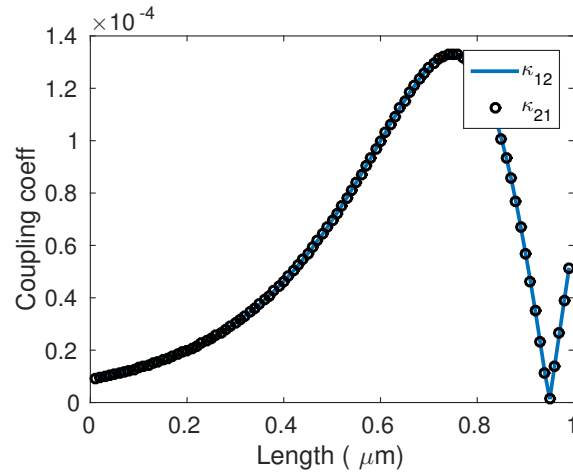

Figure 4.5: Coupling coefficients κ_{12} and κ_{21} versus normalized length.

If we do the simulation for a adiabatic structure with the same exact geometry but without bending; $\rho(z) = 0 \; \forall z$ we needed a length of at least $\sim 200\mu m$. Now the length for the bend structure will be $\sim 7\mu m$.
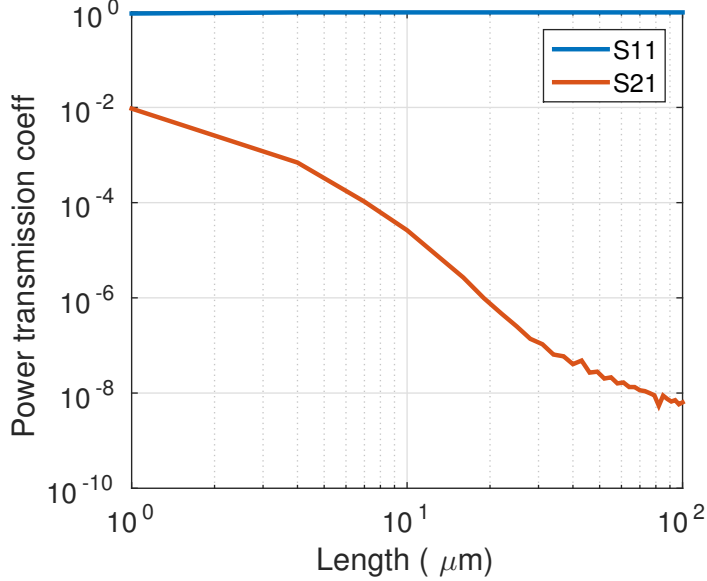

Figure 4.6: Power transferred from mode one to mode one and power transferred form mode one to mode two versus length of the device.

4.1.2 The physical interpretation

In this subsection we will give an intuitive way to understand the physical interpretation of the coupler. As we seen everything is related to the coupling coefficient from Eq. 3.10. The key thing to notice is that the Eq.3.10 it is integrated over the cross section. So the term

$$\frac{\partial n(x,y)^2}{\partial z}$$

will only be non-zero if the structure changes along z. The body of the waveguide does not contribute on the coupling coefficient but only the sidewalls do. This is because the derivative term inside the integral. The body of the waveguide is constant and so the derivative term is only non-zero at the sidewalls. As we can see on Figure 4.7 a) the coupling coefficient is zero since the sidewalls do not

change along z. The coupling sign of the coefficient can be obtained just by multiplying the sign of the first mode, second mode and the derivatives at the sidewalls. We can obtain the sign of the derivative term by looking at Figure 4.7. For example for structure b) the sign of the derivative term for the top sidewall will be positive since it goes from a lower refractive index to a higher refractive index. If the sidewall slope gets steeper then the derivative term will get higher. Looking at Figure 4.7 b) and c) we get a positive and negative coupling coefficient, respectively. Figure 4.7 d) it is a taper. It has vertical symmetry and we can see how the coupling coefficient is zero.
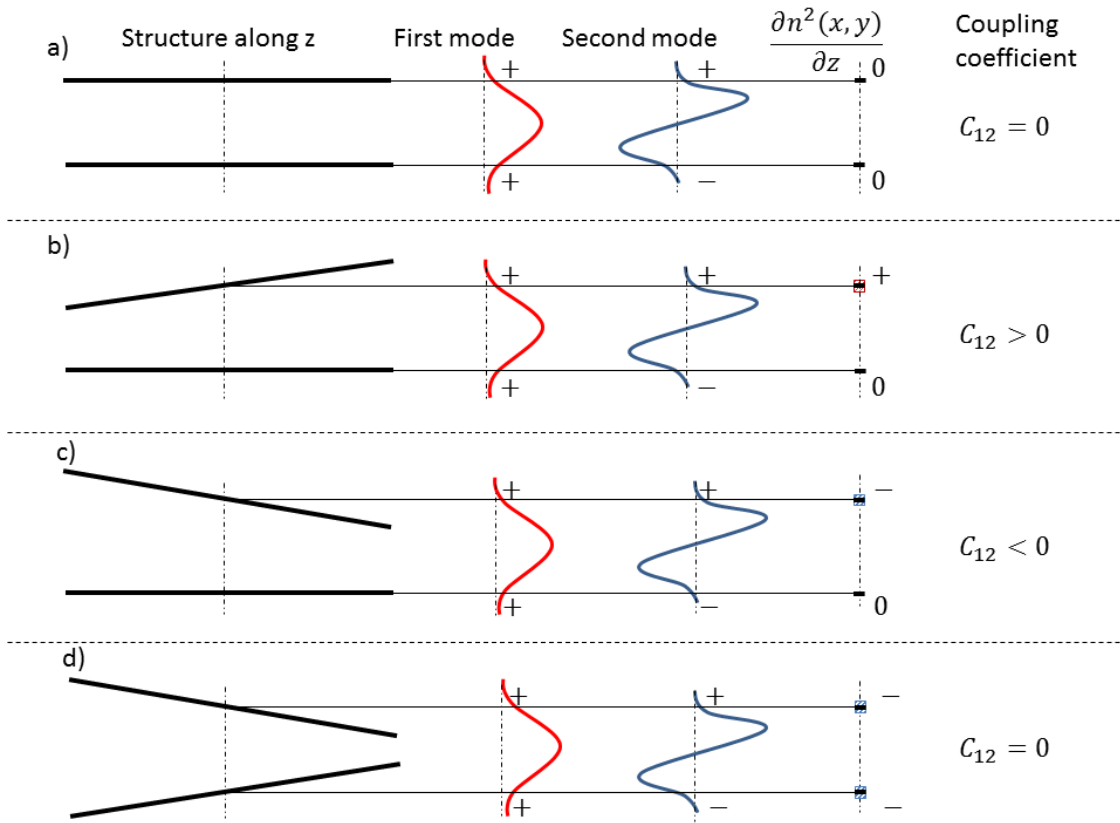

Figure 4.7: In a,b,c,d we can see different configurations of a single waveguide. The difference is how we tilt the walls. We apply local mode theory at the center cross section to compute the coupling coefficient from Eq. 3.10.

Now we consider two waveguides, one wider than the other. We have four walls to consider. In Figure 4.8 a) and b) we can see the same geometry but changing the sign of the tilting angle.

This yields to the same coupling coefficient with different signs. So there must be a tilt point in between that provides zero coupling. In this case it happens to be the trivial case where the structure is straight, but in structures where the walls are not parallel this is still the case, even though there is no angle at which all four walls are straight.
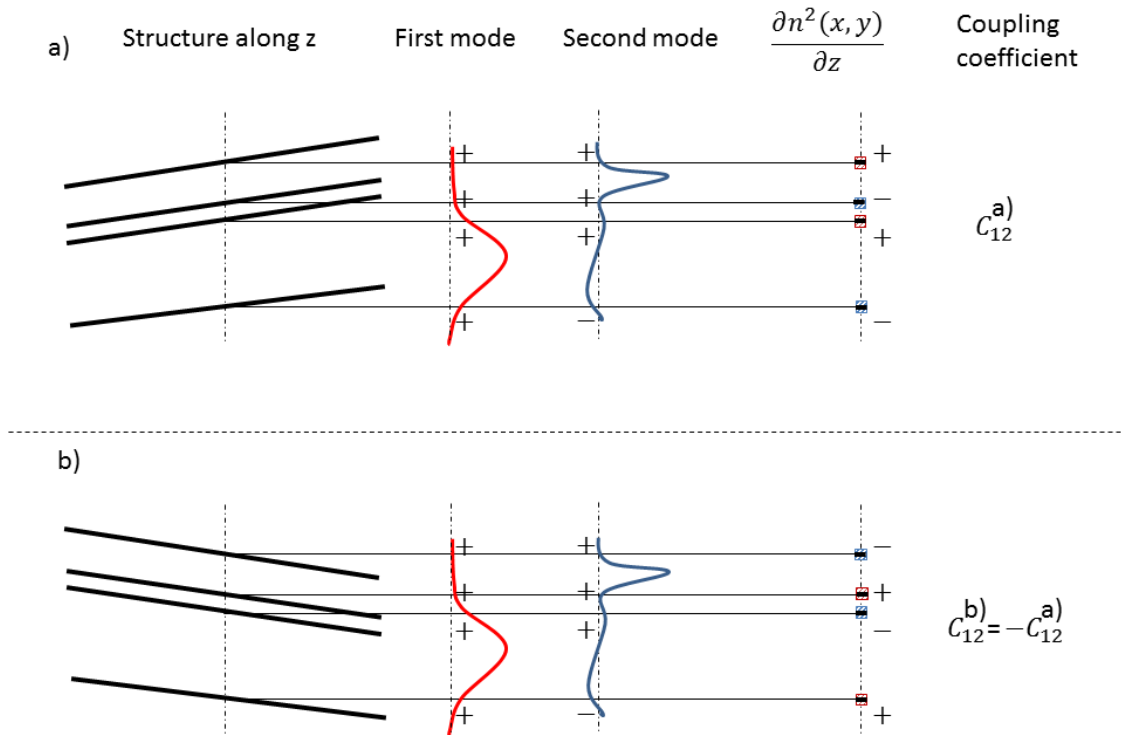

Figure 4.8: In a,b we can see different configurations of two waveguides. The difference is how we tilt the walls. We apply local mode theory at the center cross section to compute the coupling coefficient from Eq. 3.10.

Finally we show how we have to multiply the values at the walls for the first field, second field and the derivative term (Figure 4.9). Then we have to integrate over all this 4 values to obtain the coupling coefficient. The values for the product of the first and second mode are fixed. Such value does not depend on the tilt. Then the value of the derivative term will be higher if the slope is more abrupt. So we have four positive and negative values that we can tweak to make

the coupling coefficient equal to zero. We would tweak those values by changing the tilt along z. Although we are suggesting using the tilt to alter the coupling coefficient, the design of the cross-section itself is already constrained by the design of the mode shape evolution (modes 1 and 2) from input to output. So, we are introducing a new (additional) design degree of freedom into adiabatic structures which has normally not been considered in literature on design of adiabatic structures (which was concerned with cross-section evolution alone).
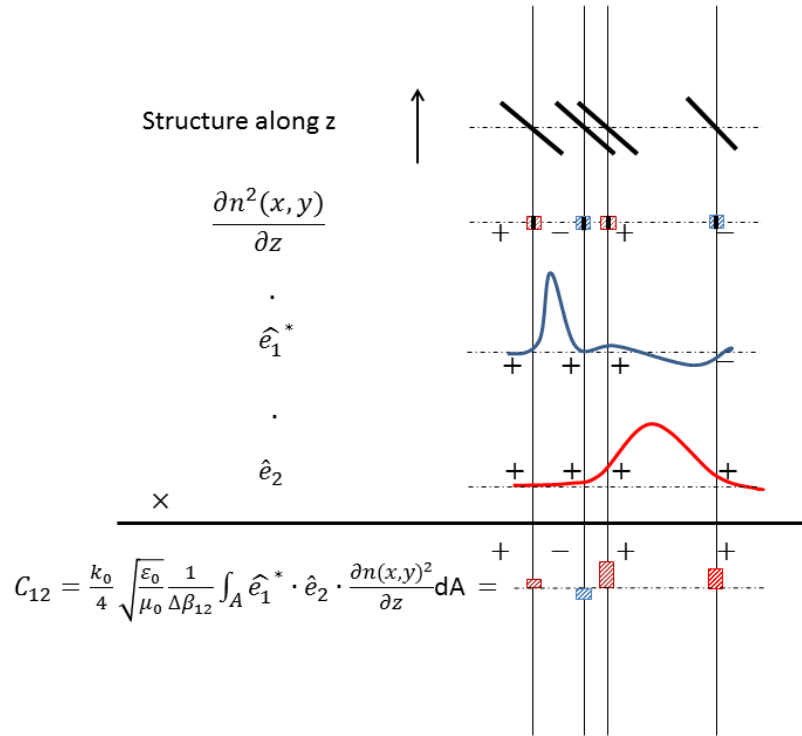

Figure 4.9: The coupling coefficient from Eq. 3.10 obtained by adding the product of the first field, second field and the derivative term at the walls.

4.1.3   2D design

Now we want to verify our designs using FDTD. We will start with a two dimensional design since it take less computational time and then we will do the three dimensional simulation. The

geometry of the two dimensional design has been chosen analogously to the third dimensional.

As it happened with the directional coupler besides of the coupling region we need an input and output regions. The output wave is easy to design and can be short since the only requirement is to have reflection symmetry. The only think we have to worry about is the curvature of the waveguides. If the bending is really abrupt we will loss light by scattering.

The input starts with two equal singlemode waveguides separated by $\sim 0.8\mu m$. We have to link up this first slice with the the first section of our coupling region. In the input region we will be changing the gap and both widths at the same time. Again, we could use an adiabatic structure to do this transition but then I can not be short. The strategy we are going to follow to design this part is similar to the one we used for the coupling region. We are going to define θ as the tilting of all the structure (similarly to Figure 4.3). So we are going to think about the input as a rigid piece that can rotate an angle θ. If we simulate the structure for different angles using FDTD2D we can see that exist an angle that minimizes the coupling between crossed modes. Even more the parameter $S12$ is less than $1e-4$ which is desired. We will not be able to use this strategy in 3D since the minimum $S12$ we can achieve is $1e-3$ which means that assuming that everything works ideally besides the input part the maximum we can achieve is 40/60 at the output.
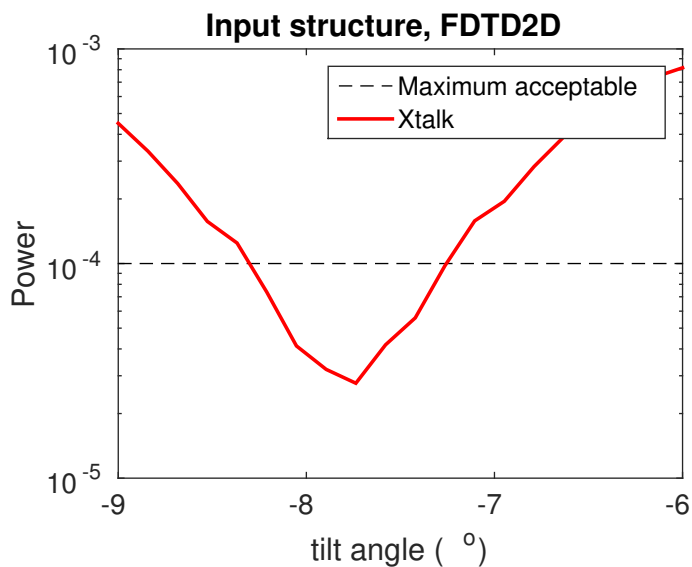
Figure 4.10: Input tilt structure.

As we can see in Figure 4.10 we want an input angle about -8 degrees. Once the input is working the design the output in the same way as the directional coupler. So we just need two symmetrical sinusoidal bends.
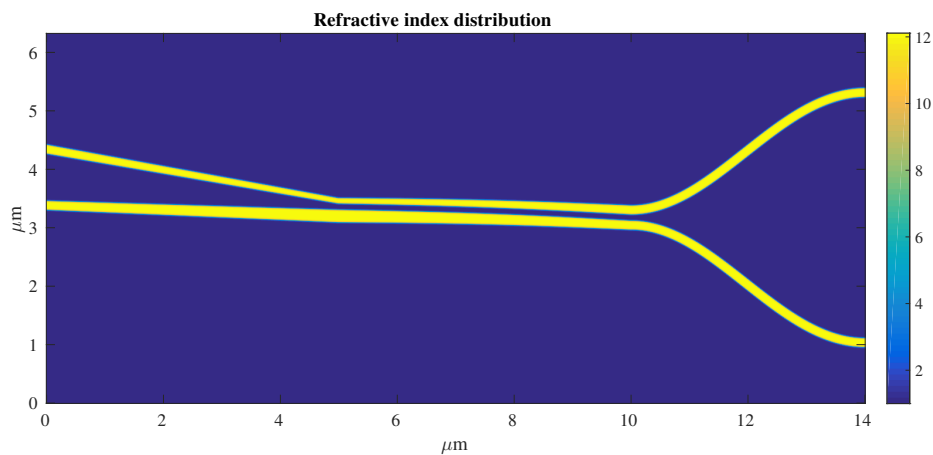

Figure 4.11: Left to right: Input region, coupling region and output region.

Then we fix the input and output size and we simulate the structure while changing the
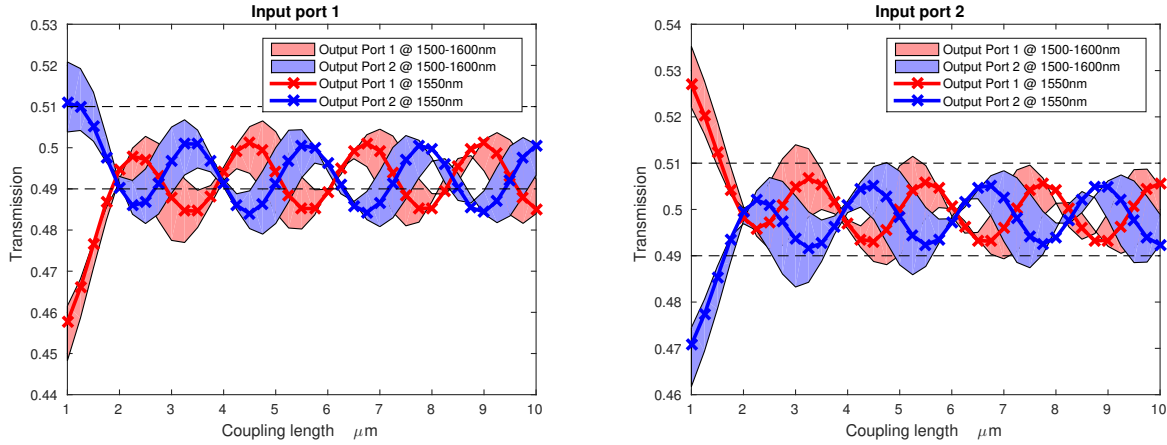
coupling region length.

Figure 4.12: Coupler performance versus device length. On the left lunching the pulse on the upper waveguide. On the right lunching the pulse on the down waveguide.

The results are promising. They oscillate with length and we can see that $L_{coupling} = 2\mu m$ gives an awesome performance.

4.1.4   3D design

The next step is simulating the 3D structure. We could think that changing form 2D to 3D is straightforward but is not. In 3D we find some problems that we had not in 2D. The first problem is the existence of two different polarizations that can couple. We already solved this problem by using SiO2 cladding. But doing that we reduced the index contrast and our design is not going to be as short as 2D. The second problem is the small gap required in 3D. This small gap yields a symmetrical mode where a lot of power is confined in the slot. Then if we are not careful when we separate the two waveguides at the output a lot of power will be radiated. We solved that problem by changing the output sine bends by splines where keeping symmetry we can play with the curvature. It turns out that if we match the slope at the ending of the coupling region with

the slope at the last section there is no power radiation. And so we can separate the power evenly. Going from two separate waveguides to an asymmetrical situation at the beginning of the coupling region is not trivial ether. The trick we used on the 2D design does not work anymore. So the input section is now the bottleneck length wise. Using splines to define this section we can optimize it to get the best performance. The final design is
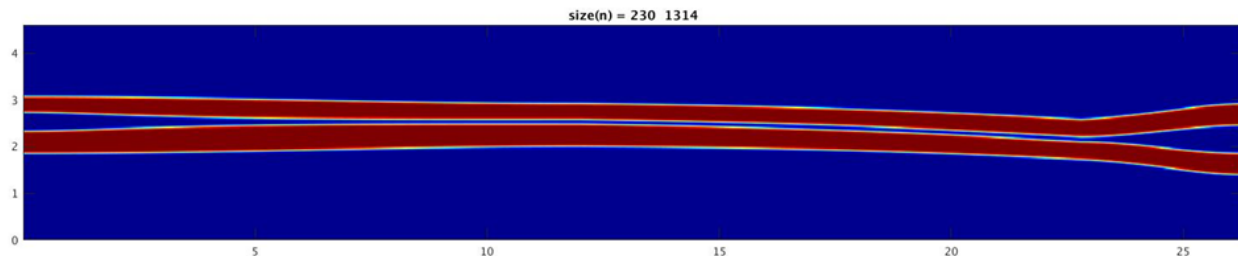

Figure 4.13: Final design dielectric; top vision.

The dimension in microns are

	Input section	Coupling section	output section
Length	12	11.8	4
Upper waveguide width	0.34	0.38	0.46
Gap	0.4	0.1	0.6
Lower waveguide width	0.48	0.38	0.46

Table 4.1: 3D design geometry

So the total length of the device is $28\mu m$. Would need an extra input to go from two 800nm separated 460nm width waveguides to the input. But this may just take 3um or less, using sinusoidal bends. After a FDTD3D analysis on this structure lunching light only for one port we get the normalized power at both outputs.
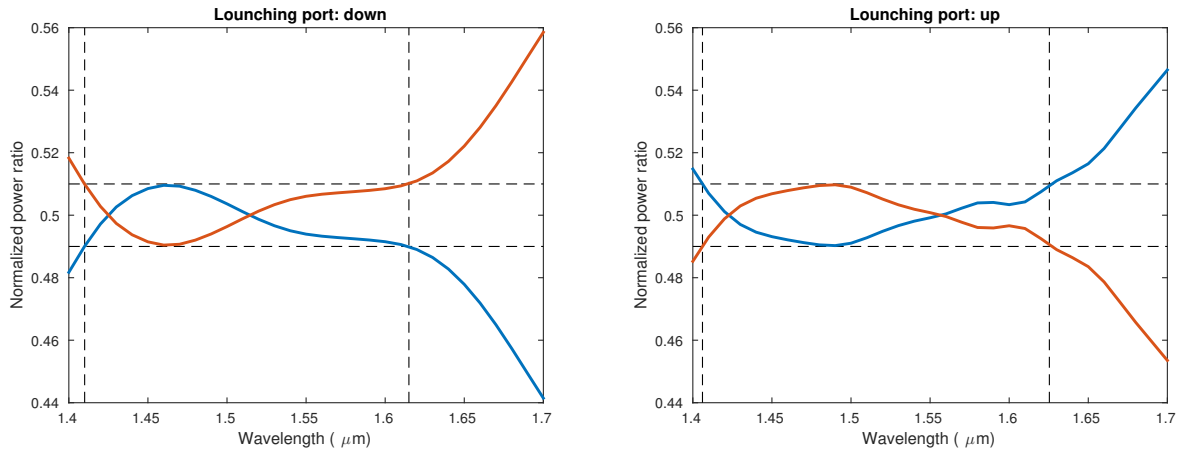
Figure 4.14: Coupler performance: Normalized power versus wavelength. On the left we are lunching the light on the down port and on the right we are lunching the light on the up port.
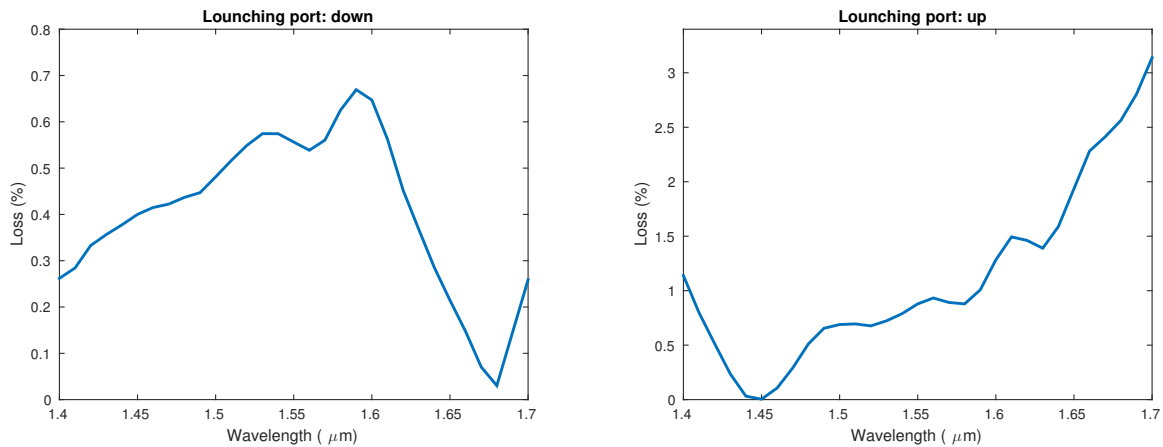
And on Figure 4.15 we show the loss:

Figure 4.15: Coupler performance: Loss versus wavelength. On the left we are lunching the light on the down port and on the right we are lunching the light on the up port.

The performance of this 2x2 coupler is astonishing.

4.1.5   Conclusion

We have demonstrated on simulation a new type of coupler called frustrated coupling based adiabatic coupler. This coupler consist on a short 2x2 adiabatic coupler. The way we can do it

so short is by cancelling the coupling from the symmetrical and antisymmetrical supermodes by bending the structure along z. The splitting ratio is really good, less than 1% along a broad range $\Delta\lambda = 205nm$. Also along this range the loss is under 1.5%.

Chapter 5

Conclusions

In this thesis we have explored the different types of 2x2 couplers on the literature. We have recapitulated the state of the art and the best results achieved by the community so far. A high-performance coupler has to be broad-band, short, lowloss and with a small power split imbalance. A directional coupler can not be high-performance since is not broadband.

Type of coupler	Bandwidth [nm]	Power split imbalance [dB]	Length [μm]
Adiabatic [4]	60 (1271-1331)	0.005	150
MMI [3]	35 (1530-1565)	0.09-0.11	152
Frustrated coupling based adiabatic coupler	205 (1420-1625)	0.174	28

Table 5.1: 2x2 couplers coparation

We put the adiabatic coupler on the table but has a 300 thick silicon cross section so the results are not comparable with a 220nm silicon cross section. The adiabatic has the better performance but if they would change the ridge waveguide for a 220 thick silicon waveguide they would have a larger structure. On the MMI design they have a power split imbalance between 0.09-0.11 dB on a 35nm band. Our design has a power split imbalance lower than 0.11 dB on a 40nm band and also a power split imbalance lower than 0.17 dB over a 205nm band as we can see in the following Figure 5.1. Also over this range the loss are lower than 1.5%. And finally the best part it is 5 times shorter.
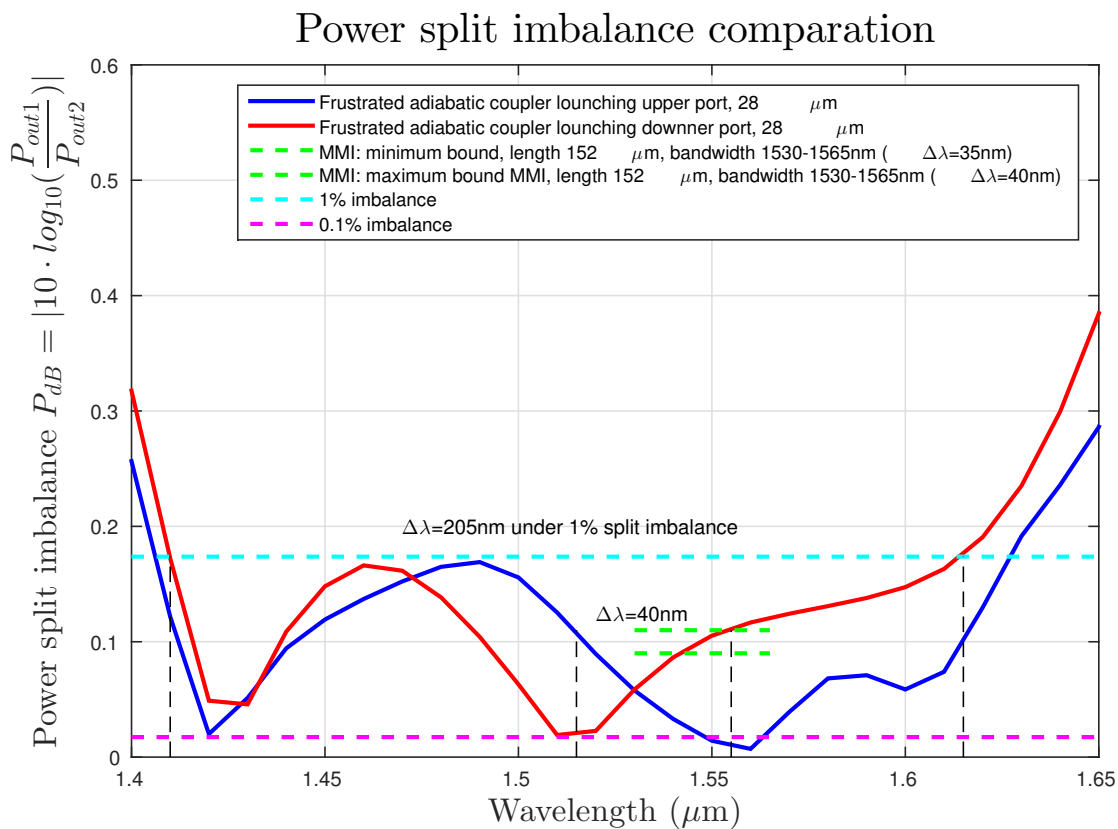
Figure 5.1: Frustrated coupling based adiabatic coupler performance and cooperation with the best MMI builded on 220nm thick silicon with SiO2 cladding so far [3].

So we can conclude that we designed the best 2x2 coupler so far. We used a completely new concept. The next step will consist on the fabrication and test of the frustrated coupling based adiabatic coupler.

Bibliography

[1] M Blahut and A Opilski. Multimode interference structures-new way of passive elements technology for photonics. Optoelectronics Review, (3):293–300, 2001.

[2] W. K. Burns and A. F. Milton. Waveguide Transitions and Junctions, pages 89–144. Springer Berlin Heidelberg, Berlin, Heidelberg, 1988.

[3] Patrick Dumais, Yuming Wei, Ming Li, Fei Zhao, Xin Tu, Jia Jiang, Dritan Celo, Dominic Goodwill, Hongyan Fu, Dongyu Geng, and eric Bernier. 2x2 multimode interference coupler with low loss using 248 nm photolithography. In Optical Fiber Communication Conference, page W2A.19. Optical Society of America, 2016.

[4] Karim Hassan, Cédric Durantin, Vincent Hugues, Bertrand Szelag, and Alain Glière. Robust silicon-on-insulator adiabatic splitter optimized by metamodeling. Appl. Opt., 56(8):2047–2052, Mar 2017.

[5] H. Kogelnik and R. Schmidt. Switched directional couplers with alternating 916; 914;. IEEE Journal of Quantum Electronics, 12(7):396–401, July 1976.

[6] Enrique AJ Marcatili. Dielectric rectangular waveguide and directional coupler for integrated optics. Bell Labs Technical Journal, 48(7):2071–2102, 1969.

[7] Stewart E. Miller. Integrated optics: An introduction. Bell System Technical Journal, 48(7):2059–2069, 1969.

[8] Raymond C. Rumpf. Lecture 5 (em21) – coupled-mode theory, Feb 2014.

[9] Yosi Shani, Charles H Henry, Rodney C Kistler, Rudolph F Kazarinov, and Kenneth J Orlowsky. Integrated optic adiabatic devices on silicon. IEEE Journal of quantum Electronics, 27(3):556–566, 1991.

[10] A.W. Snyder and J. Love. Optical Waveguide Theory. Science paperbacks. Springer US, 1983.

[11] Copyright. In Dietrich Marcuse, editor, Theory of Dielectric Optical Waveguides (Second Edition), pages iv –. Academic Press, second edition edition, 1991.

[12] Jiejiang Xing, Kang Xiong, Hao Xu, Zhiyong Li, Xi Xiao, Jinzhong Yu, and Yude Yu. Silicon-on-insulator-based adiabatic splitter with simultaneous tapering of velocity and coupling. Opt. Lett., 38(13):2221–2223, Jul 2013.